

Quantum Correlations, Entanglement, and Squeezed States of Light in Kerr Optical Frequency Combs

Yanne K. Chembo*

*FEMTO-ST Institute [CNRS UMR6174], Optics Department,
15B Avenue des Montboucons, 25030 Besançon cedex, France.*

(Dated: August 7, 2022)

The dynamical behavior of Kerr optical frequency combs is very well understood today from the perspective of the semi-classical approximation. In this article, we provide a theoretical understanding of the phenomena of quantum correlations, multimode entanglement and squeezed states of light that can occur in these frequency combs when quantum noise is accounted for. We prove that for all stationary spatio-temporal patterns, the side-modes that are symmetrical relatively to the central (pumped) mode in the frequency domain display quantum correlations that can lead to squeezed states of light under some optimal conditions that are analytically determined. We show that these quantum correlations can persist regardless the dynamical state of the system (rolls or solitons), regardless of the spectral extension of the comb (number sidemodes), and regardless of the dispersion regime (normal or anomalous). We study with particular emphasis the two principal architectures for Kerr comb generation, namely the add-through and add-drop configurations. We show that in both cases, the ratio between out-coupling and total losses plays a key role as it directly determines the efficiency of the squeezing. We also explicitly determine the phase quadratures leading to photon entanglement, and analytically calculate their quantum noise spectra. The relevance of Kerr combs for quantum information systems at optical telecommunication wavelengths is also discussed.

PACS numbers: 03.65.Ud, 42.50.Dv, 42.50.Lc, 42.65.Sf

I. INTRODUCTION

Kerr optical frequency combs are sets of equidistant spectral lines that are generated after pumping a whispering gallery mode (WGM) or ring resonator with a continuous-wave (cw) laser [1–3]. When the bulk resonator has both an ultra-high quality factor and a Kerr nonlinearity, it can at the same time trap the pump photons for a significantly long time in the torus-like modes of the resonator, and host the nonlinear interactions amongst them. Above a certain threshold, these confined and long-lifetime pump photons are transferred through four-wave mixing (FWM) to neighboring cavity-modes, provided that phase-matching, energy and momentum conservation conditions are fulfilled. This process can be further cascaded and yield a frequency comb with all-to-all coupling, and involving up to several hundred modes over several THz. In comparison to optical frequency comb generators based on femtosecond mode-locked lasers, Kerr comb generators are fairly simple, compact, robust and energy-efficient: they are expected to be a core photonic systems for many applications, such as integrated photonics, metrology, aerospace and communication engineering [4–13].

Beyond these potential applications, which have been a very powerful drive, Kerr comb are also actually an ideal test-bench systems for fundamental physics, and particularly, for quantum optics. In fact, understanding Kerr comb generation is strikingly simple when one consid-

ers the photon picture and describes the process as the photonic interaction $\hbar\omega_m + \hbar\omega_p \rightarrow \hbar\omega_n + \hbar\omega_q$, where two input photons m and p interact coherently via the Kerr nonlinearity to yield to output photons n and q . Without further analysis, this interpretation already suggests that purely quantum phenomena based on the non-classical nature of light can eventually arise in Kerr combs.

From a theoretical point of view, it is well known today that in the semi-classical limit, Kerr combs can be described using either a set of coupled ordinary differential equations (one equation per mode [14–16]), or using a single partial differential equation (one equation for the sum of the modes [17–19]). It is also well known that both formalisms are in fact perfectly equivalent [18], with the first one emphasizing the spectro-temporal dynamics of the system, while the second emphasizes the spatio-temporal dynamics. It is important to note here that these Kerr comb models are singularly accurate: the comparison between the numerical power spectra obtained using the models and the experimental ones is excellent across a dynamical range that can be as large as 80 dB [14, 20–22].

The spatio-temporal formalism is generally known as the Lugiato-Lefever equation (LLE), and was introduced for the first time by Lugiato and Lefever in the context of ring resonators where the semi-classical cavity fields were subjected to Kerr nonlinearity and diffraction [23]. In the approximation of 1D-diffraction, some of the key dynamical properties of this optical system had also been derived in the same article, such as for example the super- and sub-critical Turing instability leading to roll patterns.

*Email address: yanne.chembo@femto-st.fr

Few years later, several researchers started to explore the quantum properties of this paradigmatic system. The first contribution along that line was proposed by Lugiato and Castelli in ref. [24]. In that work, they have demonstrated that in the approximation of 1D-diffraction, the two main oscillating sidemodes which generate roll patterns are correlated twin beams, in the sense that their intensity difference exhibits fluctuations below the standard quantum noise limit (QNL). This important result, which for the first time predicted squeezing in optical systems ruled by the LLE, was obtained in the three-mode approximation (central pumped mode and two sidemodes), and therefore, was only valid close to the threshold leading to the rolls in the super-critical case. Zambrini *et al.* numerically showed later on that the squeezing behavior when certain additional degrees of freedom are accounted for is still consistent with the one of the reduced three-mode truncation [25].

Further research on the quantum properties of optical systems ruled by the LLE was performed with the more realistic case of 2D-diffraction. However, in that case, the roll pattern is unstable and instead, the simplest non-trivial solution is a hexagonal structure which emerges through a sub-critical bifurcation. As a consequence, the number of modes involved in the dynamics increases significantly because of the hexagonal structure itself (the smallest order truncation now involves 7 modes, instead of 3 for the roll pattern), and because of its sub-critical nature (the higher-order sidemodes can not be legitimately discarded anymore, even close to threshold, so that even the 7-modes truncation is not very accurate). However, using that lowest-order truncation, Grynberg and Lugiato had shown very early that that these hexagons can display four-fold mode squeezing in a lossless cavity close to threshold [26], while Gatti and Mancini have extended the results and shown that squeezing and multimode entanglement persists even in the presence of losses, and even far above threshold as long as the 7-mode truncation remains a good approximation [27].

In view of these preceding results, it could therefore be foreshadowed that Kerr combs, which can be described with great accuracy by the LLE in the semi-classical limit, can display a non-classical behavior as well. In this regard, an elegant demonstration of the theoretical prediction of Lugiato and Castelli has been achieved recently: in the experiment reported in ref. [28], squeezing in a Kerr comb is experimentally demonstrated between the two-sidemodes of a 15th-order roll pattern. Most important, this experiment is also the very first demonstration of squeezing in Kerr optical frequency combs, to the best of our knowledge.

The LLE used to model Kerr combs has an essential dissimilarity with the one initially introduced by Lugiato and Lefever: diffraction is replaced by dispersion. This difference is of no importance from the mathematical point of view. However, from the physical standpoint,

the difference is significant. On the one hand, Kerr comb generation is genuinely 1D, originates from a small bulk cavity (from μm - to mm-size), and involves guided fields: the system is experimentally compact, simple, low-power, versatile, controllable, and its behavior can be described by the LLE with high accuracy as emphasized above despite its high dimensionality (from three to up to several hundred modes). On the other hand, in the initial system, the approximation of 1D diffraction is rather poor (the 2D approximation is much better), the fields are propagating freely, and the cavity is set up with mirrors: the system is experimentally very complex and the LLE is a rather simplistic model, even though the number of interacting modes is always very limited (rarely more than 10).

From a purely technical point of view, other important points to consider are the central frequency of the comb, its spectral span, and the frequency separation between the comb lines. Even though some works have shown that the combs can be obtained with a pump close to the lower and upper limits of the near-infrared range (~ 800 nm [29] and ~ 2500 nm [30]), the overwhelming majority Kerr combs are generated today with laser pumps around 1550 nm. Since this wavelength corresponds to the well known telecom spectral window, there is a plethora of commercial off-the-shelf optical components (lasers, photodiodes, narrow filters, amplifiers, phase shifters, etc.) that are available for the manipulation of the photons around that wavelength, even at the single-photon level. It is also noteworthy that many nonlinear amorphous and crystalline materials have low dispersion and losses in that wavelength window, and these are two features that are of extreme importance in Kerr comb generation.

Moreover, Kerr combs originate from an hyper-parametric process: hence, the frequency separation between the spectral lines generally ranges from 1 to 100 GHz for the Kerr combs of interest, instead of ~ 100 THz for parametric processes. Hence, in Kerr combs, the down-converted signals fall into the microwave range where there is a very wide variety of technological solutions for the careful handling of low-noise signals.

For the above reasons, Kerr combs have many singular advantages for quantum optics experiments, powered by the possibility to manipulate the photons in the optical frequency domain, and measure their slowly-varying attributes (amplitude and phase) in the microwave frequency domain. They also have the potential to play a major role in compact or integrated quantum-information systems at optical telecommunication wavelengths [31–33].

Despite the aforementioned theoretical works in the context of quantum phenomena of LLE-based systems, and despite the promising technological opportunities highlighted above, several critical problems remain wide open for the understanding of the quantum properties of

Kerr optical frequency combs.

A first challenge is that in the literature, the available research results to this date only consider minimally truncated expansions, whose validity is automatically restricted to a parameter range close to threshold. However, Kerr combs are generally operated far above threshold, and can be very large – up to several hundreds of modes. They can also correspond to a different kind of spatiotemporal patterns such as rolls (super- and sub-critical) or solitons (bright and dark), for example. It is therefore important to investigate in detail the quantum correlations in the case of Kerr combs where spectrum amplitude, size and span restrictions do not apply.

A second issue is related to the sources of quantum noise in the system. Previous theoretical works on LLE-based systems focused on gedanken experiments where the unique source of losses was the semi-reflecting mirror used to couple the light in and outside the cavity (the intrinsic losses were null). The corresponding equations therefore included only one vacuum fluctuation term. However, in the case of Kerr combs, the resonators are bulk, and then, necessarily lossy. This introduces an extra term related to vacuum fluctuations induced by these intrinsic losses. Actually, the in- and out-coupling processes might also be distinct (like in the add-drop configuration, for example), so that overall, we might have up to three vacuum fluctuation terms, instead of just one. In order to remain close to the experimental reality, it is therefore necessary to understand the effect at the quantum level between all these intrinsic and extrinsic vacuum fluctuations.

The third open point is the explicit determination of the quadratures that can potentially lead to multimode squeezing. The conjugate variable of the photon number operator is the phase operator [34], so that when the squeezing occurs for the a linear combination of modal intensities, there exists necessarily a corresponding linear combination of correlated phase quadratures in the system. In Kerr combs, the large number of modes and the complexity of the all-to-all coupling amongst them allows for a large variety of phase-locking patterns in the semi-classical limit: the determination of the equivalent quantum correlations in terms of phase quadratures is therefore of particular relevance.

Our objective is to provide answers to the three open points highlighted above, and the article is therefore organized as follows. In the next section, we present a brief overview of the mean-field models used to model the dynamics of Kerr combs in the semi-classical limit. Important physical considerations such as orders of magnitudes and system architecture will be discussed in detail. In Sec. III, we build the quantum models for Kerr combs, using both the canonical quantization and the Hamiltonian formalism. Particular emphasis will be laid on the various sources of quantum noise that have to be accounted for depending on the in- and out-coupling configuration. Quantum correlations and squeezing for the photon numbers is investigated in Sec. IV, where we will explain why

the squeezing properties of the comb are degraded as the size of the comb increases. Section V is devoted to the study of the quantum correlations and squeezing behavior in both the amplitude and phase quadratures, after the explicit derivation of the relevant quantum Langevin equations. Particular emphasis is laid on the analysis of squeezing in rolls and solitons (bright and dark), which are the most prevalent spatiotemporal patterns in Kerr comb generation, and their squeezing spectra will be investigated in Sec. VI. We resume our main results in the last section, which concludes this article.

II. SEMI-CLASSICAL MODELS FOR KERR OPTICAL FREQUENCY COMBS

We provide here a brief overview of the semi-classical models for Kerr combs, which are useful to gain a deep understanding of the quantum models that will be developed in the next section, and which are also needed to introduce the key macroscopic parameters needed to describe the system.

A. Modal expansion model

WGM resonators, as well as ring-resonators, generally have several families of longitudinal (azimuthal) modes [35–37]. Let us consider that only one family is involved in our case, and without loss of generality, we also consider that it is the fundamental family (torus-like modes). In that case, the modes of interest, which are sometimes referred to as azimuthal, can be unambiguously defined by a single integer wavenumber ℓ , which characterizes each member's angular momentum. In the case of WGM resonators, this number ℓ can be considered as equal to the total number of reflections that a photon undergoes during one round trip in the cavity (ray-optics interpretation). Let us also consider that the eigennumber of the mode that is pumped by the external laser is ℓ_0 . In the spectral neighborhood of ℓ_0 , the eigenfrequencies of the resonator can be expanded in a Taylor series, following

$$\omega_\ell = \omega_{\ell_0} + \sum_{n=1}^{n_{\max}} \frac{\zeta_n}{n!} (\ell - \ell_0)^n, \quad (1)$$

where ω_{ℓ_0} is the eigenfrequency at $\ell = \ell_0$ and n_{\max} is the order of truncation for the expansion.

For a disk resonator with main radius a , the parameter $\zeta_1 = c/n_g a = \Delta\omega_{\text{FSR}}$ stands for the free-spectral range (FSR), with c being the velocity of light and n_g the group-velocity refraction index at ω_{ℓ_0} . This intermodal angular frequency is, of course, linked to the round-trip period of a photon through the resonator as $T_{\text{FSR}} = 2\pi/\zeta_1$. The parameter ζ_2 stands for the second-order group-velocity dispersion of the eigenmodes (normal GVD for $\zeta_2 < 0$, and anomalous GVD when $\zeta_2 > 0$).

We recall that ζ_2 is generally the sum of two contributions, namely the geometrical dispersion (normal) and the material dispersion (normal or anomalous). The parameters ζ_n for $n \geq 2$ stand for higher-dispersion terms and in this study, these terms will be considered as uniformly null. Note that perfect equidistance for the eigenfrequencies is achieved when $\zeta_n \equiv 0$ for all $n \geq 2$. More details can be found in refs. [14, 15, 18, 38], for example.

The resonator is also characterized by its losses, which can be internal or external. For each mode, the internal losses (bulk absorption, surface scattering, etc.) are quantified by the linewidth $\Delta\omega_{\text{int},\ell}$. On the other hand, the external losses $\Delta\omega_{\text{ext},\ell}$ are here considered to be induced by both the in- or out-coupling processes of the optical fields. The total losses are just defined as the sum of the two aforementioned contributions following $\Delta\omega_{\text{tot},\ell} = \Delta\omega_{\text{int},\ell} + \Delta\omega_{\text{ext},\ell}$. The loaded (or total) Q factor for each mode can be defined as $Q_{\text{tot},\ell} = \omega_\ell / \Delta\omega_{\text{tot},\ell}$, and the modal photon lifetime is $\tau_{\text{ph},\ell} = 1 / \Delta\omega_{\text{tot},\ell}$.

The total electric field inside the cavity can be expanded as

$$\mathbf{E}(\mathbf{r}, t) = \sum_{\ell} \frac{1}{2} \mathcal{A}_{\ell}(t) e^{i\omega_{\ell} t} \mathbf{r}_{\ell}(\mathbf{r}) + \text{c.c.} \quad (2)$$

where t is the time, $\mathcal{A}_{\ell}(t)$ is the complex-valued slowly-varying amplitude of the ℓ -th mode, $\mathbf{r}_{\ell}(\mathbf{r})$ is the corresponding spatial mode profile, and c.c. stands for the “complex conjugate” of all the preceding terms. It is important to note that in Eq. (2), and the fields have been normalized such that $|\mathcal{A}_{\ell}|^2$ is equal to the number of photons in the ℓ -th mode.

It has been shown in ref. [15] that the slowly varying envelopes \mathcal{A}_{ℓ} of the modes are governed by the following system of equations:

$$\begin{aligned} \frac{d\mathcal{A}_{\ell}}{dt} = & -\frac{1}{2} \Delta\omega_{\text{tot},\ell} \mathcal{A}_{\ell} + \frac{1}{2} \Delta\omega_{\text{tot},\ell} \mathcal{F}_{\ell} e^{i\sigma t} \delta(\ell - \ell_0) \quad (3) \\ & -ig_0 \sum_{\ell_m, \ell_n, \ell_p} \mathcal{A}_{\ell_m} \mathcal{A}_{\ell_n}^* \mathcal{A}_{\ell_p} e^{i(\omega_{\ell_m} - \omega_{\ell_n} + \omega_{\ell_p} - \omega_{\ell})t} \\ & \times \Lambda_{\ell}^{\ell_m \ell_n \ell_p} \delta(\ell_m - \ell_n + \ell_p - \ell), \end{aligned}$$

where $\delta(x)$ is the Kronecker delta-function that equals 1 when $x = 0$ and equals zero otherwise. In the above equation, the Kronecker functions indicate that only the mode $\ell = \ell_0$ is pumped, and that the allowed four-wave mixing interactions will be those for which the total angular momentum of the interacting photons is conserved, following $\ell_m + \ell_p = \ell_n + \ell$.

The four-wave mixing gain is $g_0 = n_2 c \hbar \omega_{\ell_0}^2 / n_0^2 V_{\text{eff}}$, where \hbar is Planck’s constant, n_2 is the Kerr coefficient at $\ell = \ell_0$, and $V_{\text{eff}} = [\int_V \|\mathbf{r}_{\ell_0}(\mathbf{r}_{\perp})\|^4 dV]^{-1}$ is the effective mode volume of the pumped mode. The parameter $\Lambda_{\ell}^{\ell_m \ell_n \ell_p}$ is an intermodal coupling tensor which weights the spatial overlap amongst the various modes. The laser pump field is characterized by the detuning $\sigma = \Omega_0 - \omega_{\ell}$ between its angular frequency $\Omega_0 = 2\pi c / \lambda_0$ and the resonance frequency ω_{ℓ_0} of the pumped mode, and by

$\mathcal{F}_{\ell_0} = [4\Delta\omega_{\text{ext},\ell_0} / \Delta\omega_{\text{tot},\ell_0}^2]^{1/2} [P / \hbar \Omega_0]^{1/2}$ which stands for the external pumping field, with $\Delta\omega_{\text{ext}}$ representing in-coupling losses only.

Equation (3) can be further simplified and rewritten in a more convenient form, suitable for the canonical quantization. The first step is to introduce the reduced eigen-number $l = \ell - \ell_0$, so that the pumped mode is now $l = 0$, while the various sidemodes symmetrically expand as $l = \pm 1, \pm 2, \dots$, with “+” and “-” standing respectively for higher and lower frequency sidemodes. The modes ℓ_m, ℓ_n and ℓ_p in the four-wave mixing sum will now be simply replaced by their reduced counterpart as $\{m, n, p\} = \ell_{\{m, n, p\}} - \ell_0$. The second step is to consider that the spectral extension of the comb is narrow enough to consider that the modes are quasi-degenerated in space and frequency ($\Lambda_l^{mnp} \equiv 1$), and that the modal losses are quasi-degenerated as well, with $\Delta\omega_l \equiv \Delta\omega_{\text{tot},0} = \Delta\omega_{\text{tot}}$. The last step is to replace the fields $\mathcal{A}_{\ell} \equiv \mathcal{A}_l$ in Eq. (3) by $\mathcal{A}_l^* \exp[i(\sigma - \frac{1}{2}\zeta_2 l^2)t]$, so that explicit time dependence is removed in Eq. (3). From a physical viewpoint, this latter transformation corresponds to setting the frequency reference at the laser frequency, and to express the modal frequencies with respect to the equidistant (FSR-spaced) frequency grid, instead of the dispersion-detuned eigenfrequency grid [39].

After implementing these mathematical transformations, it can be shown that the new modal fields \mathcal{A}_l obey the following set of autonomous, nonlinear and coupled ordinary differential equations:

$$\begin{aligned} \dot{\mathcal{A}}_l = & -\frac{1}{2} \Delta\omega_{\text{tot}} \mathcal{A}_l + i \left[\sigma - \frac{1}{2} \zeta_2 l^2 \right] \mathcal{A}_l \\ & + \delta(l) \sqrt{\Delta\omega_{\text{ext}}} \mathcal{A}_{\text{in}} \\ & + ig_0 \sum_{m, n, p} \delta(m - n + p - l) \mathcal{A}_m \mathcal{A}_n^* \mathcal{A}_p. \quad (4) \end{aligned}$$

where the overdot indicates the time derivative. Without loss of generality, we can arbitrarily consider the phase of the external pump field as a reference and set it to zero, so that this field becomes real-valued and can be written as

$$\mathcal{A}_{\text{in}} = A_{\text{in}} = \sqrt{\frac{P}{\hbar \Omega_0}}. \quad (5)$$

It is important to recall the normalization in the semiclassical Eqs. (4) is such that $|\mathcal{A}_l|^2$ is a number of photons (cavity fields), while $|A_{\text{in}}|^2$ is a number of photons per second (propagating fields). This normalization is physically the most appropriate at the time to perform the canonical quantization. Note that a necessary (but not sufficient) condition on the pump field to trigger Kerr comb generation is

$$|A_{\text{in}}|^2 > \frac{\Delta\omega_{\text{tot}}^3}{8g_0 \Delta\omega_{\text{ext}}}. \quad (6)$$

This minimal value, which is obtained for $\sigma = -\frac{1}{2}\Delta\omega_{\text{tot}}$ in the anomalous dispersion regime (see refs. [15, 39]),

gives an order of magnitude of the photon flux needed to excite a comb.

B. The two configurations under study

Two configurations are routinely used to generate Kerr optical frequency combs. It is therefore important to identify precisely all the loss terms as well as the out-coupled fields in each case, because as we will see later on, the vacuum quantum noise terms are closely related to these losses and out-coupling configurations.

In the first architecture, that we call *add-through* [40], a single coupler is used to pump the cavity and to retrieve the comb signal, which is detected at the through port. This architecture allows for limited coupling losses (and therefore, low threshold power for Kerr comb generation). However, a disadvantage of this architecture is that the output signal is a superposition of the intra-cavity and a portion of the pump which is directly passing through the coupling waveguide [20]. In this add-through configuration, the total and external linewidths in Eq. (4) can be written as

$$\Delta\omega_{\text{tot}} \equiv \Delta\omega_{\text{int}} + \Delta\omega_{\text{ext},t} \quad (7)$$

$$\Delta\omega_{\text{ext}} \equiv \Delta\omega_{\text{ext},t}, \quad (8)$$

while the modal output fields obey

$$\mathcal{A}_{\text{out},l} = \sqrt{\Delta\omega_{\text{ext},t}} \mathcal{A}_l - A_{\text{in}}\delta(l). \quad (9)$$

with $\Delta\omega_{\text{ext},t}$ standing for the coupling losses in the through port.

In the second architecture, referred to as *add-drop*, two different couplers are used to perform in- and out-coupling tasks. The comb is therefore retrieved at the drop port. This double-coupling has the disadvantage to increase the overall losses (thereby increasing the threshold for Kerr comb generation), but however, at the opposite of the precedent case, the output signal is proportional to the intra-cavity field and provides an unambiguous representation of the physical processes that are taking place inside the resonator. For the add-drop configuration, the linewidths in Eq. (4) are explicitly defined as

$$\Delta\omega_{\text{tot}} \equiv \Delta\omega_{\text{int}} + \Delta\omega_{\text{ext},t} + \Delta\omega_{\text{ext},d} \quad (10)$$

$$\Delta\omega_{\text{ext}} \equiv \Delta\omega_{\text{ext},t}, \quad (11)$$

and the modal output fields simply obey

$$\mathcal{A}_{\text{out},l} = \sqrt{\Delta\omega_{\text{ext},d}} \mathcal{A}_l. \quad (12)$$

where $\Delta\omega_{\text{ext},d}$ stands for the coupling losses in the drop port [41].

In all cases, the various linewidths are related to their corresponding quality factors by $\Delta\omega_{\text{int,ext,tot}} = \Omega_0/Q_{\text{int,ext,tot}}$. A technique routinely used to determine the various quality factors at the experimental level is the cavity-ring-down method [42].

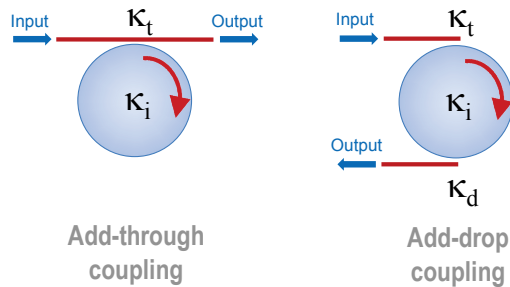


FIG. 1: (Color online) The two main configurations for Kerr comb generation with monolithic resonators, namely the add-through and add-drop configurations. Each architecture features a certain number of loss mechanisms (quantified by their linewidths $\kappa_{t,i,d}$), which are associated to vacuum fluctuations. The related quantum noise contributions have to be accounted for when calculating the squeezing spectra.

C. Spatiotemporal formalism

Several studies on the quantum properties of self-organized dissipative optical structures are performed on systems that are ruled by the LLE. In the case of Kerr combs, it has been shown in ref. [18] that the above modal expansion model is exactly equivalent to the following LLE

$$\frac{\partial\psi}{\partial\tau} = -(1 + i\alpha)\psi + i|\psi|^2\psi - i\frac{\beta}{2}\frac{\partial^2\psi}{\partial\theta^2} + F \quad (13)$$

where $\psi(\theta, \tau) = (2g_0/\Delta\omega_{\text{tot}})^{1/2} \sum_l \mathcal{A}_l(\tau) e^{il\theta}$ is the total intra-cavity field, $\theta \in [-\pi, \pi]$ is the azimuthal angle (along the circumference of the resonator), and $\tau = \Delta\omega_{\text{tot}}t/2 = t/2\tau_{\text{ph}}$ is the dimensionless time. The dimensionless parameters of this normalized equation are the frequency detuning $\alpha = -2\sigma/\Delta\omega_{\text{tot}}$, the cavity second-order dispersion $\beta = -2\zeta_2/\Delta\omega_{\text{tot}}$, and the external excitation $F = (8g_0\Delta\omega_{\text{ext},t}/\Delta\omega_{\text{tot}}^3)^{1/2} \sqrt{P/\hbar\Omega_0}$. In the context of Kerr comb generation, the LLE, has been extensively investigated in several articles.

In ref. [39], an exhaustive study of the various dynamical regimes has been performed, and the stability basin of the various solutions has been determined. In the anomalous dispersion regime, the stationary solutions are rolls (super- and sub-critical), bright solitons (isolated or coexisting), and soliton molecules (isolated or coexisting). In the case of normal dispersion, the stationary solutions can be rolls, and dark solitons (isolated or coexisting). For all these stationary solutions, the Kerr comb is perfectly symmetric in the semi-classical limit, and we will see in Sec. IV that this symmetry opens the way for multimode squeezing when quantum noise is accounted for.

D. Orders of magnitude in experimental systems

In order to facilitate comparisons between theory and experiments, it is important to link the normalized parameters and variables to their counterparts in SI units. In particular, knowing the power levels involved provides key information at the time to choose the low-noise, high sensitivity components needed to perform experiments with non-classical light [43].

In our Eq. (4), the dispersion parameter ζ_2 is linked to the parameter β_2 used in fiber optics by $\beta_2 = -\zeta_2/v_g\Delta\omega_{\text{FSR}}^2$ (in s^2m^{-1}), where $v_g = c/n_g$ is the group velocity. The coefficient g_0 can be converted to the non-linear coefficient $\gamma = \Omega_0 n_2 / c A_{\text{eff}} = g_0 T_{\text{FSR}} / v_g \hbar \Omega_0$ (in $\text{W}^{-1}\text{m}^{-1}$) which is also well known in fiber optics, where $A_{\text{eff}} = V_{\text{eff}} / 2\pi a$ is the effective area which can be approximated by $A_{\text{eff}} \simeq 0.35 (\lambda_0 / n_g)^{\frac{7}{6}} a^{\frac{5}{6}}$ for a spherical WGM resonator (this is generally a higher bound estimate for WGM disks or ring resonators). Finally, the intra-cavity and output dimensionless intensities $|\mathcal{A}_l|^2$ and $|\mathcal{A}_{\text{out},l}|^2$ can be converted in watts following $|\mathcal{E}_l|^2 = \hbar \Omega_0 |\mathcal{A}_l|^2 / T_{\text{FSR}}$ and $|\mathcal{E}_{\text{out},l}|^2 = \hbar \Omega_0 |\mathcal{A}_{\text{out},l}|^2$.

The theory based on the stability analysis of the LLE indicates that Kerr combs can scarcely be generated when the normalized intra-cavity power $|\psi|^2$ and external pump power F^2 are inferior to 1: the equivalent absolute minimum powers in watts needed to trigger Kerr comb generation are therefore

$$|\mathcal{E}_{\text{min}}|^2 = \frac{\hbar \Omega_0}{2g_0} \frac{\Delta\omega_{\text{tot}}}{T_{\text{FSR}}} = \frac{\Delta\omega_{\text{tot}}}{2\gamma v_g} \quad (14)$$

$$P_{\text{min}} = \frac{\hbar \Omega_0}{8g_0} \frac{\Delta\omega_{\text{tot}}^3}{\Delta\omega_{\text{ext},t}} = \frac{T_{\text{FSR}}}{8\gamma v_g} \frac{\Delta\omega_{\text{tot}}^3}{\Delta\omega_{\text{ext},t}}, \quad (15)$$

respectively. we recall that the above values are absolute minima, that can be reached when the laser is accurately detuned to $\sigma = -\frac{1}{2}\Delta\omega_{\text{tot}}$ in the anomalous dispersion regime. For any other detuning, and in both dispersion regimes, the threshold power for Kerr comb generation will necessarily be higher, up to a factor 100 [39].

Therefore, for mm-size crystalline resonator with 10 GHz free-spectral range ($T_{\text{FSR}} = 100$ ps), $\gamma \sim 1 \text{ W}^{-1}\text{km}^{-1}$, $n_g \sim 1.4$, and $Q_{\text{int}} = Q_{\text{ext}} \sim 10^9$ at 1550 nm in the add-through configuration, the absolute minimum threshold power can be as low as $P_{\text{min}} \sim 1$ mW. Such low pumping power have already been demonstrated experimentally, like in ref. [44] where a threshold power of ~ 2 mW was sufficient to trigger Kerr comb generation. On the other hand, for an integrated silicon nitride resonator with 100 GHz repetition rate, $\gamma \sim 10 \text{ W}^{-1}\text{km}^{-1}$, $n_g \sim 2$, and quality factors $Q_{\text{int}} = Q_{\text{ext}} \sim 3 \times 10^6$ at 1550 nm in the add-through configuration, the absolute minimum threshold pump power is rather $P_{\text{min}} \sim 1$ W.

III. QUANTUM MODEL FOR KERR OPTICAL FREQUENCY COMBS

The determination of the dynamical behavior of the Kerr comb at the quantum level can be performed through the canonical quantization of the semi-classical model, or by defining an Hamiltonian operator ruling the relevant interactions in the system. The first approach has the advantage to be more intuitive, while the second is generally helpful at the time to establish conservation rules (which are closely related to commutators involving the Hamiltonian). In the present article we will use both formalisms, which will be introduced in this section to derive the temporal behavior of the Kerr comb.

A. Canonical quantization

The canonical quantization permits to derive the quantum counterpart of a semi-classical model, and in our case it consists in three steps [45, 46]: (i) replace all the fields $\mathcal{A}_l(t)$ and their complex conjugates $\mathcal{A}_l^*(t)$ by annihilation and creation operators $\hat{a}_l(t)$ and $\hat{a}_l^\dagger(t)$, respectively [47]; (ii) introduce vacuum fluctuation operators for every loss mechanism (intrinsic or extrinsic) in the optical system; (iii) introduce vacuum fluctuation operators at both the in- and out-coupling ports.

The creation and annihilation operators obey the following boson commutation rules

$$[\hat{a}_l, \hat{a}_{l'}^\dagger] = \delta_{l,l'} \quad (16)$$

$$[\hat{a}_l, \hat{a}_{l'}] = [\hat{a}_l^\dagger, \hat{a}_{l'}^\dagger] = 0. \quad (17)$$

The semi-classical photon number $|\mathcal{A}_l|^2 = \mathcal{A}_l^* \mathcal{A}_l$, which was a measure of the intra-cavity optical energy for each mode, is now represented by its quantum counterpart, which is the photon number operator

$$\hat{n}_l = \hat{a}_l^\dagger \hat{a}_l. \quad (18)$$

It is useful to recall that the ordering of the operators \hat{a}_l^\dagger and \hat{a}_l can not be arbitrarily swapped, as these two operators do not commute. We adopt here the so-called normal ordering which consists in placing the creation operators on the left and the annihilation operators on the right. Also note that the total intra-cavity field is described by the operator

$$\hat{a}(\theta, t) = \sum_l \hat{a}_l(t) e^{i l \theta}, \quad (19)$$

and its Hermitian conjugate.

The vacuum fluctuations associated to losses and coupling can be explicitly introduced in each mode using the vacuum operators $\hat{V}_{i,l}$ for the intrinsic losses, $\hat{V}_{t,l}$ for the coupling losses in the through port, and $\hat{V}_{d,l}$ for the coupling losses in the drop port. These free-field operators have zero-mean value and obey the commutation rules

$$[\hat{V}_{s,l}(t), \hat{V}_{s',l'}^\dagger(t')] = \delta_{s,s'} \delta_{l,l'} \delta(t - t'), \quad (20)$$

where s, s' = t (through), i (intrinsic), or d (drop). Let us also introduce the following notation for the sake of conciseness:

$$2\kappa_i \equiv \Delta\omega_{\text{int}} \quad (21)$$

$$2\kappa_d \equiv \Delta\omega_{\text{ext,d}} \quad (22)$$

$$2\kappa_t \equiv \Delta\omega_{\text{ext,t}} \quad (23)$$

$$2\kappa \equiv \Delta\omega_{\text{tot}}. \quad (24)$$

The pumping field is now defined as a coherent state

$$\hat{A}_{\text{in}} = A_{\text{in}} + \hat{V}_{t,0}. \quad (25)$$

which is the sum a semi-classical (real-valued) contribution, and a vacuum fluctuation that will be inserted in the through port. Its commutation rules is therefore

$$[\hat{A}_{\text{in}}(t), \hat{A}_{\text{in}}^\dagger(t')] = [\hat{V}_{t,0}(t), \hat{V}_{t,0}^\dagger(t')] = \delta(t - t'), \quad (26)$$

and it therefore has the same quantum-noise properties as a vacuum fluctuation.

The quantum canonization can be now be performed by transforming the semi-classical Eqs. (4), (9) and (12) into their quantum counterparts.

For the add-through configuration, the quantum model explicitly reads

$$\begin{aligned} \dot{\hat{a}}_l &= -\kappa \hat{a}_l + i \left[\sigma - \frac{1}{2} \zeta_2 l^2 \right] \hat{a}_l + \delta(l) \sqrt{2\kappa_t} A_{\text{in}} \\ &+ ig_0 \sum_{m,n,p} \delta(m - n + p - l) \hat{a}_n^\dagger \hat{a}_m \hat{a}_p \\ &+ \sqrt{2\kappa_t} \hat{V}_{t,l} + \sqrt{2\kappa_i} \hat{V}_{i,l} \end{aligned} \quad (27)$$

with

$$\kappa = \kappa_t + \kappa_i \quad (28)$$

$$\hat{A}_{\text{out},l} = \sqrt{2\kappa_t} \hat{a}_l - A_{\text{in}} \delta(l) - \hat{V}_{t,l}. \quad (29)$$

On the other hand, for the add-drop configuration, the quantum model is therefore

$$\begin{aligned} \dot{\hat{a}}_l &= -\kappa \hat{a}_l + i \left[\sigma - \frac{1}{2} \zeta_2 l^2 \right] \hat{a}_l + \delta(l) \sqrt{2\kappa_t} A_{\text{in}} \\ &+ ig_0 \sum_{m,n,p} \delta(m - n + p - l) \hat{a}_n^\dagger \hat{a}_m \hat{a}_p \\ &+ \sqrt{2\kappa_t} \hat{V}_{t,l} + \sqrt{2\kappa_i} \hat{V}_{i,l} + \sqrt{2\kappa_d} \hat{V}_{d,l}. \end{aligned} \quad (30)$$

where the losses and the output field operator obey

$$\kappa = \kappa_t + \kappa_i + \kappa_d \quad (31)$$

$$\hat{A}_{\text{out},l} = \sqrt{2\kappa_d} \hat{a}_l - \hat{V}_{d,l}. \quad (32)$$

Note that because of the normal ordering, the creation operator in the nonlinear interaction terms is always placed on the left. Also, in the canonical quantization procedure, the pump fields A_{in} have not been explicitly replaced by the operator \hat{A}_{in} , since the related vacuum fluctuation $\sqrt{2\kappa_t} \hat{V}_{t,0}$ is already accounted for in the generic term $\sqrt{2\kappa_t} \hat{V}_{t,l}$.

B. Hamiltonian formalism

The theoretical understanding of the quantum properties of Kerr optical frequency combs can also be achieved through an Hamiltonian formalism, and in our case, the total Hamiltonian of the system has three contribution.

The first contribution corresponds to the propagation of the fields, following

$$\begin{aligned} \hat{H}_{\text{free}} &= \hbar \int_{-\pi}^{+\pi} \hat{a}^\dagger \left[\sigma + \frac{1}{2} \zeta_2 \frac{\partial}{\partial \theta^2} \right] \hat{a} d\theta \\ &= \hbar \sum_l \left[\sigma - \frac{1}{2} \zeta_2 l^2 \right] \hat{a}_l^\dagger \hat{a}_l. \end{aligned} \quad (33)$$

The second contribution originates from the external pump field, and reads

$$\hat{H}_{\text{ext}} = i\hbar\sqrt{2\kappa_t} A_{\text{in}} \left(\hat{a}_0^\dagger - \hat{a}_0 \right). \quad (34)$$

The third and last contribution comes from the interactions related to the Kerr nonlinearity:

$$\begin{aligned} \hat{H}_{\text{int}} &= -\frac{1}{2} \hbar g_0 \int_{-\pi}^{+\pi} (\hat{a}^\dagger)^2 (\hat{a})^2 d\theta \\ &= -\frac{1}{2} \hbar g_0 \sum_{m,n,p,q} \delta(m - n + p - q) \hat{a}_n^\dagger \hat{a}_q^\dagger \hat{a}_m \hat{a}_p. \end{aligned} \quad (35)$$

For the physical understanding of the quantum phenomena in Kerr media, it is sometimes useful to decompose the interaction Hamiltonian itself into three contributions following

$$\hat{H}_{\text{int}} = \hat{H}_{\text{SPM}} + \hat{H}_{\text{CPM}} + \hat{H}_{\text{FWM}}, \quad (36)$$

where

$$\hat{H}_{\text{SPM}} = -\frac{1}{2} \hbar g_0 \sum_m (\hat{a}_m^\dagger)^2 (\hat{a}_m)^2 \quad (37)$$

is the self-phase modulation (SPM) contribution (a single mode is involved in the interaction),

$$\hat{H}_{\text{CPM}} = -2\hbar g_0 \sum_{n < m} (\hat{a}_n^\dagger)^2 (\hat{a}_m)^2 \quad (38)$$

is the cross-phase modulation (CPM) contribution (two distinct modes are involved), while the four-wave mixing (FWM) term \hat{H}_{FWM} gathers all the remaining monomials of \hat{H}_{int} , which necessarily involve three or four distinct interacting modes.

The total Hamiltonian is therefore

$$\hat{H}_{\text{tot}} = \hat{H}_{\text{free}} + \hat{H}_{\text{ext}} + \hat{H}_{\text{int}}, \quad (39)$$

and it is interesting to note that this Hamiltonian can be very large for Kerr combs. In earlier studies related to quantum correlations in systems ruled by the LLE, the Hamiltonian was always truncated to a maximum of few

tens of monomials. However, in our case, if we consider a comb with $l = -K, \dots, K$ (that is, a comb with $2K + 1$ modes), then the interaction Hamiltonian \hat{H}_{int} has exactly $\frac{1}{3}[2(2K + 1)^3 + (2K + 1)]$ monomials: this number therefore grows in a cubic polynomial fashion with the number of modes, and for a comb with ~ 100 modes, there is already $\sim 10^6$ monomials in the Hamiltonian.

The Hamiltonian \hat{H}_{tot} can now be used to track the temporal dynamics of the quantum Kerr comb, as it permits to obtain an explicit equation for the annihilation operator \hat{a}_l following

$$\dot{\hat{a}}_l = \frac{1}{i\hbar} [\hat{a}_l, \hat{H}_{\text{tot}}] + \sum_s \left[-\kappa_s \hat{a}_l + \sqrt{2\kappa_s} \hat{V}_{s,l} \right]. \quad (40)$$

where the index s runs across the various loss terms corresponding to the configuration under study, that is

$$s = \begin{cases} \text{t, i} & \text{for add-through} \\ \text{t, i, d} & \text{for add-drop} \end{cases}, \quad (41)$$

The term $\kappa = \sum_s \kappa_s$ stands for the total losses [see Eqs. (7) and (10)], and $\hat{V}_{s,l}$ represent the vacuum fluctuations corresponding to these losses. On the other hand, the output field is

$$\hat{A}_{\text{out},l} = \sqrt{2\kappa_r} \hat{a}_l - A_{\text{in}} \delta_{t,r} \delta(l) - \hat{V}_{r,l}. \quad (42)$$

where the index r stands for the output port following

$$r = \begin{cases} \text{t} & \text{for add-through} \\ \text{d} & \text{for add-drop} \end{cases}. \quad (43)$$

Equation (40) is identical to Eqs. (27) and (30), and the output field operators defined in Eq. (42) in the add-through and add-drop configurations obey the same relationships as in Sec. III A. The commutator $[\hat{a}_l, \hat{H}_{\text{tot}}]$ generates exactly $3K^2 + 3K - l^2 + 1$ monomials, and accordingly, Eq. (40) includes a large number of terms as well. We also note that this formalism is close to the one adopted by Matsko *et al.* to investigate the temporal dynamics of Kerr combs in the deterministic regime, that is, when all the vacuum noise terms are uniformly set to zero [48].

Another approach is to study the following Master Equation [24]:

$$\dot{\hat{\rho}} = \sum_l \Lambda_l \hat{\rho} - \frac{1}{i\hbar} [\hat{\rho}, \hat{H}_{\text{tot}}]. \quad (44)$$

where $\hat{\rho}$ is the density operator for the comb, and Λ_l is a Liouvillian explicitly defined as

$$\Lambda_l = [\hat{a}_l \hat{\rho}, \hat{a}_l^\dagger] + [\hat{a}_l, \hat{\rho} \hat{a}_l^\dagger]. \quad (45)$$

In this article, we will however only consider the Hamiltonian in the context of Eq. (40), which yields a set of equations that are formally identical to those obtained through the canonical quantization in Sec. III A.

IV. QUANTUM CORRELATIONS AND SQUEEZING FOR THE PHOTON NUMBERS

In the frequency comb corresponding to a stationary pattern like rolls of solitons, the photon number in each semi-classical sidemodes is defined as $|\mathcal{A}_{\text{out},\pm l}|^2 = N_{\text{out},\pm l}$, which is proportional to the optical power that can be photo-detected experimentally for each of these to modes. We have recalled in Sec. II C that for being symmetrical, both side-modes have the same amplitude, their photon numbers are equal and the average intensity difference $\langle N_{\text{out},\Delta} \rangle = \langle N_{\text{out},l} \rangle - \langle N_{\text{out},-l} \rangle$ is null in the semi-classical limit. This result indicates that the quantum operator corresponding to this difference in photon numbers could potentially display a noticeably non-classical behavior under optimal conditions.

Here, we show that in a stationary Kerr comb (rolls or solitons), the photon number difference $N_{\text{out},\Delta} = N_{\text{out},l} - N_{\text{out},-l}$ which experimentally corresponds to difference of optical powers photo-detected for the modes $+l$ and $-l$ can under certain conditions display squeezing. We also show that this squeezing can be observed not only for rolls close to threshold within a three-modes approximation, but also for any type of stationary Kerr comb, regardless of the number of modes involved and the dispersion regime, and even far above threshold.

A. General case of combs with arbitrary number of modes

Let us then consider the modal photon number operators $\hat{n}_l = \hat{a}_l^\dagger \hat{a}_l$ and $\hat{n}_{-l} = \hat{a}_{-l}^\dagger \hat{a}_{-l}$, which correspond to the modes $+l$ and $-l$, respectively. From the Heisenberg Eq. (40), we can determine the time-domain dynamics of these operators as

$$\begin{aligned} \dot{\hat{n}}_{\pm l} &= \hat{a}_{\pm l}^\dagger \dot{\hat{a}}_{\pm l} + \dot{\hat{a}}_{\pm l}^\dagger \hat{a}_{\pm l} \\ &= -2\kappa \hat{n}_{\pm l} + \frac{1}{i\hbar} [\hat{n}_{\pm l}, \hat{H}_{\text{tot}}] \\ &\quad + \sum_s \sqrt{2\kappa_s} (\hat{V}_{s,\pm l}^\dagger \hat{a}_{\pm l} + \hat{a}_{\pm l}^\dagger \hat{V}_{s,\pm l}). \end{aligned} \quad (46)$$

with $s = \text{t, i}$ for the add-through configuration, and $s = \text{t, i, d}$ for the add-drop configuration. It can be demonstrated that the photon numbers $\hat{n}_{\pm l}$ do not commute with the Hamiltonian \hat{H}_{tot} .

We can Eqs. (46) to show that the operator

$$\hat{n}_\Delta = \hat{n}_{+l} - \hat{n}_{-l} \quad (47)$$

standing for the photon number difference obeys the following time-domain equation:

$$\dot{\hat{n}}_\Delta = -2\kappa \hat{n}_\Delta + \frac{1}{i\hbar} [\hat{n}_\Delta, \hat{H}_{\text{tot}}] + \sum_s \sqrt{2\kappa_s} \hat{G}_s, \quad (48)$$

where

$$\hat{G}_s = \hat{V}_{s,+l}^\dagger \hat{a}_{+l} + \hat{a}_{+l}^\dagger \hat{V}_{s,+l} - \hat{V}_{s,-l}^\dagger \hat{a}_{-l} - \hat{a}_{-l}^\dagger \hat{V}_{s,-l}. \quad (49)$$

The expected values related to \hat{G}_s are

$$\langle \hat{G}_s(t) \rangle = 0 \quad (50)$$

$$\langle \hat{G}_s(t) \hat{G}_{s'}(t') \rangle = \langle \hat{n}_\Sigma \rangle \delta_{s,s'} \delta(t-t'), \quad (51)$$

where

$$\hat{n}_\Sigma = \hat{n}_{+l} + \hat{n}_{-l} \quad (52)$$

is the photon number operator for the sum of of the side-modes $\pm l$ [27].

In the general case, Eq. (48) ruling the dynamics of the photon number difference is highly nonlinear. However, it degenerates to a linear Langevin equation when \hat{n}_Δ commutes with \hat{H}_{tot} . In particular, this condition is fulfilled when the photon number individually commutes with \hat{H}_{free} , \hat{H}_{ext} and \hat{H}_{int} .

It is not difficult to show that \hat{n}_Δ commutes with both \hat{H}_{free} and \hat{H}_{ext} . However, the determination of the commutator $[\hat{n}_\Delta, \hat{H}_{\text{int}}]$ is much less trivial. More explicitly, using the relationships

$$[\hat{n}_{\pm l}, \hat{H}_{\text{int}}] = [\hat{a}_{\pm l}^\dagger, \hat{H}_{\text{int}}] \hat{a}_{\pm l} + \hat{a}_{\pm l}^\dagger [\hat{a}_{\pm l}, \hat{H}_{\text{int}}], \quad (53)$$

we can derive an explicit expression of the commutator $[\hat{n}_\Delta, \hat{H}_{\text{int}}]$, following

$$\begin{aligned} [\hat{n}_\Delta, \hat{H}_{\text{int}}] &= [\hat{n}_{+l}, \hat{H}_{\text{int}}] - [\hat{n}_{-l}, \hat{H}_{\text{int}}] \\ &= \hbar g_0 \sum_{n,p,q} \hat{a}_n^\dagger \hat{a}_q^\dagger \hat{a}_p \{ \delta(l-n+p-q) \hat{a}_l \\ &\quad - \delta(l+n-p+q) \hat{a}_{-l} \} - \text{H. c.} \end{aligned} \quad (54)$$

where H. c. stands for the Hermitian conjugate of all preceding terms. In fact, by setting $p \equiv q$, it can be shown that $[\hat{n}_\Delta, \hat{H}_{\text{SPM}}]$ and $[\hat{n}_\Delta, \hat{H}_{\text{CPM}}]$ are both null regardless of the size of the comb. However, $[\hat{n}_\Delta, \hat{H}_{\text{FWM}}]$ is not necessarily null. This implies that the photon number difference is generally not a conserved quantity. For example, for a 5-modes comb (let's consider $l = -2, \dots, +2$ for the sake of simplicity), the photonic interaction $2\hbar\omega_{-1} \rightarrow \hbar\omega_0 + \hbar\omega_{-2}$ induces a loss of 2 photons in the mode $l = -1$ (in favor of the modes $l = 0$ and $l = -2$), while its symmetric sidemode counterpart $l = 1$ remains unaffected. Hence, despite the fact that $\langle N_\Delta \rangle = \langle N_l \rangle - \langle N_{-l} \rangle$ is expected to be null (in average) in the semi-classical approximation, the value of N_Δ itself is not necessarily conserved at the photon level. This phenomenology can be witnessed whenever the size of the comb is larger than 5.

However, when the size of the comb is reduced to 3, the photon number *does* commute with the interaction Hamiltonian, and therefore, is conserved. This case corresponds to the problem that was originally investigated by Lugiato and Castelli in ref. [24]. From a physical

standpoint, the explanation of this feature is that in a 3-modes Kerr combs, any variation of photon number in one sidemode *must* induce the very same variation in the other sidemode. Therefore, in this case, the photon number difference itself $N_\Delta = N_l - N_{-l}$ (and not only its average value) is *strictly* null in deterministic photon picture. As a consequence, in 3-modes Kerr combs, non-classical light can be generated in twin-beams, as analyzed in the next sub-section.

B. Particular case of combs with 3 modes (pump, signal and idler)

We aim here to derive the output spectra of the photon-number difference in both the add-through and add-drop configurations, when the Kerr comb is constituted with only 3 modes. Such combs arise for example close to threshold after a super-critical Hamiltonian-Hopf bifurcation ($\sigma > -\frac{41}{60} \Delta\omega_{\text{tot}}$; see refs. [23, 39, 54]). They correspond to the so-called Turing patterns (or rolls) in the time-domain, and to primary combs in the frequency-domain. The modes can be labelled as $l = 0, \pm L$, where L is strictly positive integer, and close to threshold, a good approximation is $L \simeq \sqrt{(2/\zeta_2)[\sigma + \Delta\omega_{\text{tot}}]}$ (see refs. [15, 20, 39]).

The photon number operators for the output fields $\pm l$ are

$$\hat{N}_{\text{out},\pm L} = \hat{A}_{\text{out},\pm L}^\dagger \hat{A}_{\text{out},\pm L} \quad (55)$$

and it can be calculated using Eqs. (29) and (32). The difference between these operators is experimentally observable and can explicitly be defined as

$$\begin{aligned} \hat{N}_{\text{out},\Delta} &= \hat{N}_{\text{out},+L} - \hat{N}_{\text{out},-L} \\ &= 2\kappa_r \hat{n}_\Delta - \sqrt{2\kappa_r} \hat{G}_r + \hat{N}_{r,\Delta}^{\text{vac}}, \end{aligned} \quad (56)$$

where

$$\hat{N}_{r,\Delta}^{\text{vac}} = \hat{V}_{r,+L}^\dagger \hat{V}_{r,+L} - \hat{V}_{r,-L}^\dagger \hat{V}_{r,-L} \quad (57)$$

is an operator representing the difference of photon numbers in the vacuum fluctuation at the out-coupling stage.

In the Fourier domain, we transform the operators as

$$\tilde{U}(\omega) = \frac{1}{\sqrt{2\pi}} \int_{-\infty}^{-\infty} \hat{U}(t) e^{i\omega t} dt. \quad (58)$$

When we consider the fact that the photon number commutes with the total Hamiltonian following $[\hat{n}_\Delta, \hat{H}_{\text{tot}}] = 0$, Eq. (48) becomes linear and can be translated in the Fourier space according to

$$\tilde{n}_\Delta(\omega) = \frac{\sum_s \sqrt{2\kappa_s} \tilde{G}_s(\omega)}{2\kappa - i\omega}, \quad (59)$$

and from Eq. (57), the Fourier spectrum of the difference in photon numbers is found to be

$$\begin{aligned}\tilde{N}_{\text{out},\Delta}(\omega) &= 2\kappa_r \tilde{n}_\Delta(\omega) - \sqrt{2\kappa_r} \tilde{G}_r(\omega) + \tilde{N}_{r,\Delta}^{\text{vac}}(\omega) \\ &= \frac{2\kappa_r}{2\kappa - i\omega} \sum_s \sqrt{2\kappa_s} \tilde{G}_s(\omega) \\ &\quad - \sqrt{2\kappa_r} \tilde{G}_r(\omega) + \tilde{N}_{r,\Delta}^{\text{vac}}(\omega).\end{aligned}\quad (60)$$

Taking into account Eq. (59), the power spectrum is therefore

$$\langle |\tilde{N}_{\text{out},\Delta}(\omega)|^2 \rangle = 2\kappa_r \langle \hat{n}_\Sigma \rangle \frac{\omega^2 + 4\kappa(\kappa - \kappa_r)}{\omega^2 + 4\kappa^2}. \quad (61)$$

Since the shot noise level is $2\kappa_r \langle \hat{n}_\Sigma \rangle$, it is useful to rewrite this spectrum under the following normalized form

$$\begin{aligned}S(\omega) &= \frac{\langle |\tilde{N}_{\text{out},\Delta}(\omega)|^2 \rangle}{2\kappa_r \langle \hat{n}_\Sigma \rangle} \\ &= 1 - \rho \frac{4\kappa^2}{\omega^2 + 4\kappa^2}\end{aligned}\quad (62)$$

where the parameter $\rho \in]0, 1]$ is the squeezing factor defined as

$$\begin{aligned}\rho &= \frac{\kappa_r}{\kappa} \\ &= \begin{cases} \kappa_t / (\kappa_t + \kappa_i) & \text{for add-through} \\ \kappa_d / (\kappa_t + \kappa_i + \kappa_d) & \text{for add-drop} \end{cases}.\end{aligned}\quad (63)$$

The spectrum described by $S(\omega)$ is an inverted Lorentzian which qualitatively displays a dip below the shot noise level close to the zero frequency. It converges to 1 at $\omega = \pm\infty$, and to $1 - \rho$ at $\omega = 0$. The parameter ρ therefore represents a direct indicator of the squeezing efficiency, as $\rho \rightarrow 1$ leads to quasi-perfect squeezing at zero frequency, while $\rho \rightarrow 0$ leads to no squeezing at all frequencies. For being the ratio between out-coupling and total losses, the squeezing parameter ρ can also be interpreted as the ratio between the number of detected photons versus the total number of annihilated photons [49]. Some squeezing spectra of the photon number difference with different values of ρ are displayed in Fig. 2, where they have been plotted as solid lines.

In Kerr comb generation, efficient squeezing ($\rho \rightarrow 1$) physically corresponds to strong over-coupling in the detection port, that is, to $\kappa_t \gg \kappa_i$ in the add-through configuration, and to $\kappa_d \gg \kappa_t, \kappa_i$ in the add-drop configuration. Therefore, ultra-low loss resonators are the most perfectly suitable for the purpose of squeezing, as ρ is anyway maximized when $\kappa_i \rightarrow 0$ (or $Q_{\text{int}} \rightarrow +\infty$). In the add-through configuration, perfect squeezing at zero frequency is even possible for an ideal cavity with null intrinsic losses, since $\rho = 1$ for $\kappa_i = 0$ [24, 27].

Around 1550 nm, the record intrinsic Q factor is 3×10^{11} with a CaF₂ resonator [50]. Intrinsic quality factors of the order of 10^9 are routinely obtained with crystalline or amorphous WGM resonators. Hence, these

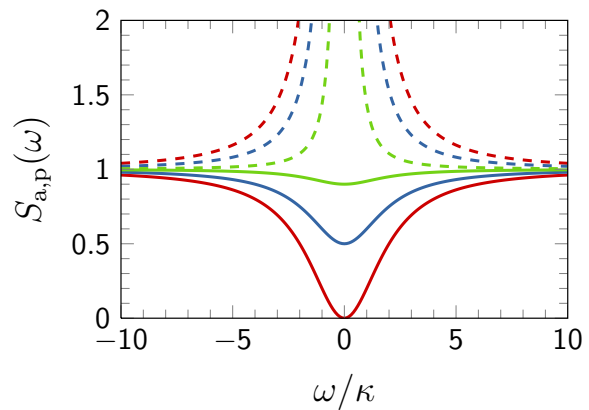


FIG. 2: (Color online) Power spectra of pure amplitude and phase quadratures for different values of the squeezing parameter ρ . The solid lines correspond to the photon number difference spectrum of Eq. (62), and to the pure amplitude quadrature spectrum of Eq. (93), since both are identical. The dashed lines correspond to the phase quadrature spectrum of Eq. (94). Green: $\rho = 0.1$; Blue: $\rho = 0.5$; Red: $\rho = 1$. We have arbitrarily set $\kappa_p \equiv \frac{1}{3}\kappa$.

ultra-low-loss resonators are therefore idoneous candidates for highly efficient squeezing, and the technological solutions for their large-scale fabrication [51], and integration in chip-scale devices [52] are already available. Finally, it is very important to note that achieving strong over-coupling in the output port ($\kappa_r \rightarrow +\infty$) is important not only to increase the efficiency of the squeezing ($\rho \rightarrow 1$), but also to increase its bandwidth ($\kappa \rightarrow +\infty$). However, one should also keep in mind that the pump power P_{min} needed to trigger comb generation will grow as κ^2 in this strongly over-coupled regime [see Eq. (15)], so that an optimal power vs bandwidth balance has to be found depending on the targeted application.

V. QUANTUM CORRELATIONS AND SQUEEZING FOR THE AMPLITUDE AND PHASE QUADRATURES

For a wide range of parameters (pump power, cavity detuning and dispersion), Kerr combs can be phase-locked and lead to the emergence of stationary spatio-temporal patterns which can be extended (rolls) or localized (solitons). Hence, beside amplitude correlations, the phase of the optical fields can display strong correlations as well.

These phase correlations at the semi-classical level can lead to phase quadrature squeezing from a quantum perspective. We hereafter determine the linearized input-output relationship that is needed to track the temporal dynamics of the modal perturbation operators under the influence of vacuum noise. This perturbation flow will allow us to determine some relevant phase quadratures

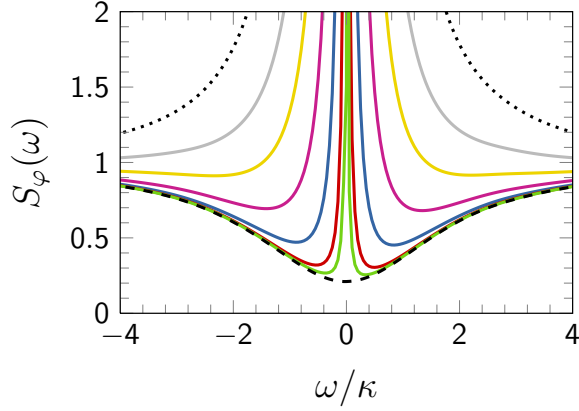


FIG. 3: (Color online) Spectra of quadratures with different angles φ in a Kerr comb close to threshold, where the 3-modes approximation is valid. The spectra are calculated using Eq. (87). The system is in the add-through configuration with $\rho = 0.8$. The threshold power is $P_{\text{th}} = 2.06$ mW and the pump power is set to $P = 1.01 P_{\text{th}}$ and the laser detuning is $\sigma = -\kappa$. The comb features sidemodes at $L = \pm 18$. Pure amplitude quadrature (dashed black) is not exactly achieved for $\varphi = \Phi$ as expected, but rather for $\varphi = \Phi + \delta\Phi \equiv \Phi_{\text{opt}}$, where $\delta\Phi$ is an additional offset angle that is generally small. In this case, we have found $\delta\Phi = 0.022$. Accordingly, pure phase quadrature (dotted black) is obtained for $\varphi = \Phi_{\text{opt}} + \frac{\pi}{2}$. The other spectra correspond to the following quadrature angles: $\varphi = \Phi_{\text{opt}} + \pi/100$ (green); $\varphi = \Phi_{\text{opt}} + \pi/50$ (red); $\varphi = \Phi_{\text{opt}} + \pi/20$ (blue); $\varphi = \Phi_{\text{opt}} + \pi/10$ (pink); $\varphi = \Phi_{\text{opt}} + \pi/6$ (yellow); $\varphi = \Phi_{\text{opt}} + \pi/4$ (gray). Note that once we deviate from the pure amplitude spectrum, we here have a divergence at zero-frequency.

for rolls, bright and dark solitons.

A. Linearized dynamics of the modal perturbation operators

Let us consider a stationary Kerr comb spanning from $l = -K$ to $l = K$ (total of $2K + 1$ modes). The intracavity modal fields can be perturbed as

$$\hat{a}_l = \mathcal{A}_l + \delta\hat{a}_l \quad (64)$$

where \mathcal{A}_l are the constant complex-valued numbers representing the semi-classical stationary states, and $\delta\hat{a}_l$ are the perturbation operators.

Then by plugging Eq. (64) into Eqs (40), it can easily be found that the steady state amplitude of the oscillating modes obey the set of $(2K + 1)$ nonlinear algebraic equations

$$-\left[\kappa - i\left(\sigma - \frac{1}{2}\zeta_2 l^2\right)\right] \mathcal{A}_l + \delta(l) \sqrt{2\kappa_t} \mathcal{A}_{in} + i g_0 \sum_{m,n,p} \delta(m - n + p - l) \mathcal{A}_n^* \mathcal{A}_m \mathcal{A}_p = 0, \quad (65)$$

while the noise driven perturbations are ruled by the following set of equations:

$$\begin{aligned} \delta\dot{\hat{a}}_l = & -\left[\kappa - i\left(\sigma - \frac{1}{2}\zeta_2 l^2\right)\right] \delta\hat{a}_l + \sum_s \sqrt{2\kappa_s} \hat{V}_{s,l} \\ & + i g_0 \sum_{m,n,p} \delta(m - n + p - l) \\ & \times \{\delta\hat{a}_n^\dagger \mathcal{A}_m \mathcal{A}_p + \mathcal{A}_n^* \delta\hat{a}_m \mathcal{A}_p + \mathcal{A}_n^* \mathcal{A}_m \delta\hat{a}_p\}. \end{aligned} \quad (66)$$

The above perturbation flow can be synthetically rewritten as

$$\delta\dot{\hat{a}}_l = \sum_{p=-K}^K \mathcal{R}_{lp} \delta\hat{a}_p + \sum_{p=-K}^K \mathcal{S}_{lp} \delta\hat{a}_p^\dagger + \sum_s \sqrt{2\kappa_s} \hat{V}_{s,l}, \quad (67)$$

where

$$\begin{aligned} \mathcal{R}_{lp} = & -\left[\kappa - i\left(\sigma - \frac{1}{2}\zeta_2 l^2\right)\right] \delta(p - l) \\ & + 2i g_0 \sum_{m,n} \delta(m - n + p - l) \mathcal{A}_m \mathcal{A}_n^* \end{aligned} \quad (68)$$

$$\mathcal{S}_{lp} = i g_0 \sum_{m,n} \delta(m + n - p - l) \mathcal{A}_m \mathcal{A}_n \quad (69)$$

can be considered as the elements of the $(2K + 1)^{\text{th}}$ -order square matrices \mathbf{R} and \mathbf{S} , and the driving quantum noise term $\sum_s \sqrt{2\kappa_s} \hat{V}_{s,l}$ represents the sum of all vacuum fluctuations for a given mode l .

If we introduce the $(2K + 1)$ -dimensional fluctuation and vacuum noise vectors

$$\delta\hat{\mathbf{a}}(t) = \begin{bmatrix} \delta\hat{a}_{-K}(t) \\ \vdots \\ \delta\hat{a}_{+K}(t) \end{bmatrix}; \quad \hat{\mathbf{V}}(t) = \begin{bmatrix} \hat{V}_{s,-K}(t) \\ \vdots \\ \hat{V}_{s,+K}(t) \end{bmatrix}, \quad (70)$$

then we can write Eq. (67) under the form of a quantum-noise-driven linear flow:

$$\begin{bmatrix} \delta\dot{\hat{\mathbf{a}}} \\ \delta\dot{\hat{\mathbf{a}}^\dagger} \end{bmatrix} = \mathbf{J}_a \begin{bmatrix} \delta\hat{\mathbf{a}} \\ \delta\hat{\mathbf{a}}^\dagger \end{bmatrix} + \sum_s \sqrt{2\kappa_s} \begin{bmatrix} \hat{\mathbf{V}}_s(t) \\ \hat{\mathbf{V}}_s^\dagger(t) \end{bmatrix}, \quad (71)$$

where

$$\mathbf{J}_a = \begin{bmatrix} \mathbf{R} & \mathbf{S} \\ \mathbf{S}^* & \mathbf{R}^* \end{bmatrix} \quad (72)$$

is a composite (block matrix) Jacobian of order $2 \times (2K + 1)$. It should be noted that this Jacobian matrix has to be determined numerically, since its components exclusively depend on the steady state values of the semi-classical modal fields \mathcal{A}_l .

B. Dynamics of the quadrature operators

Quadratures operators are observables of particular interest for the study of the quantum properties of multi-mode fields. They are Hermitian operators that correspond to linear combinations of annihilation and creation

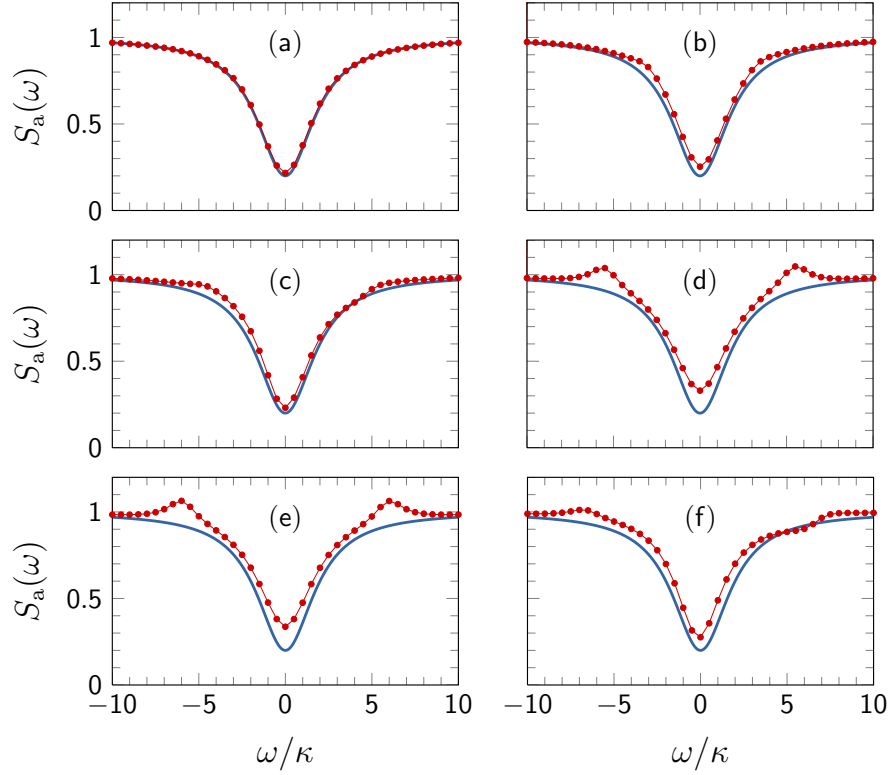


FIG. 4: (Color online) Spectra of amplitude quadratures as the pump power is increased in a Kerr comb originating from a roll pattern. Except the pump power P , the parameters of the system are the same as in Fig. 3. The modes $\pm L$ of interest are the first (main) sidemodes of the comb. The solid blue lines stand for the analytical and ideal amplitude squeezing spectrum provided by the 3-modes approximation in Eq. (93). The red dots stand for the numerical spectra obtained with Eq. (87), where all the modes of the comb are accounted for [53]. The figures display the best squeezing spectra for the pump powers P , oscillating modes $\pm L$, and offsets $\delta\Phi$ listed hereafter. (a): $P = 1.01 P_{\text{th}}$ ($L = 18$ and $\delta\Phi = 0.015$); (b): $P = 1.1 P_{\text{th}}$ ($L = 19$ and $\delta\Phi = -0.03$); (c): $P = 1.5 P_{\text{th}}$ ($L = 22$ and $\delta\Phi = 0.1$); (d): $P = 2.0 P_{\text{th}}$ ($L = 24$ and $\delta\Phi = 0.02$); (e): $P = 2.5 P_{\text{th}}$ ($L = 25$ and $\delta\Phi = -0.0025$); (f): $P = 3.0 P_{\text{th}}$ ($L = 26$ and $\delta\Phi = 0.18$). As the pump is increased, the 3-modes approximation becomes less and less valid, but very efficient squeezing can still be achieved with the fundamental pair of sidemodes.

operators, and usually, the relevant linear combinations can be inferred from the conserved quantities in the semi-classical limit.

In the case of Kerr combs, it is known that in the asymptotic limit, the amplitudes two symmetric modes $-l$ and $+l$ are equal ($|\mathcal{A}_{+l}| = |\mathcal{A}_{-l}|$), and the sum of their phases is a constant, following

$$\phi_l + \phi_{-l} = \text{Const} = 2\Phi_l. \quad (73)$$

The constant Φ_l depends on the modes $\pm l$ under consideration, but not on the initial conditions. In other words, once a symmetric pair of modes has been chosen, the sum of its steady-state slowly-varying phases is a constant of motion.

From a quantum perspective, the corresponding quadratures are

$$\delta\hat{q}_{\varphi,l} = \frac{1}{\sqrt{2}}(\delta\hat{a}_{+l} - \delta\hat{a}_{-l})e^{-i\varphi} + \text{H. c.}, \quad (74)$$

with $l = -K, \dots, K$. It is therefore interesting to investigate the dynamics of all the quadratures $\delta\hat{q}_{\varphi,l}$ altogether.

For this purpose, we can build the K -dimensional operator

$$\delta\hat{\mathbf{q}}_{\varphi} = \begin{bmatrix} \delta\hat{q}_{\varphi,1} \\ \vdots \\ \delta\hat{q}_{\varphi,L} \end{bmatrix} \quad (75)$$

with $l = 1, \dots, K$, and from Eq. (74), it is found that the vectorial quadrature $\delta\hat{\mathbf{q}}_{\varphi}$ can be rewritten as

$$\delta\hat{\mathbf{q}}_{\varphi} = \delta\hat{\mathbf{q}}_0 \cos \varphi + \delta\hat{\mathbf{q}}_{\frac{\pi}{2}} \sin \varphi \quad (76)$$

where $\delta\hat{\mathbf{q}}_0$ and $\delta\hat{\mathbf{q}}_{\frac{\pi}{2}}$ are the amplitude and phase vectorial quadratures, respectively.

The dynamics of these quadratures can be obtained from Eq. (74) as

$$\begin{aligned} \delta\dot{\hat{\mathbf{q}}}_0 &= \frac{1}{\sqrt{2}}(\delta\dot{\hat{a}}_{+l} - \delta\dot{\hat{a}}_{-l}) + \text{H. c.} \\ \delta\dot{\hat{\mathbf{q}}}_{\frac{\pi}{2},l} &= -\frac{i}{\sqrt{2}}(\delta\dot{\hat{a}}_{+l} - \delta\dot{\hat{a}}_{-l}) + \text{H. c.} \end{aligned} \quad (77)$$

Using Eqs. (71), it can be demonstrated that the amplitude and phase vectorial quadrature operators obey the closed form Langevin equation:

$$\begin{bmatrix} \delta \dot{\hat{\mathbf{q}}}_0 \\ \delta \dot{\hat{\mathbf{q}}}_{\frac{\pi}{2}} \end{bmatrix} = \mathbf{J}_{\mathbf{q}} \begin{bmatrix} \delta \hat{\mathbf{q}}_0 \\ \delta \hat{\mathbf{q}}_{\frac{\pi}{2}} \end{bmatrix} + \sum_s \sqrt{2\kappa_s} \begin{bmatrix} \hat{\mathbf{W}}_{s,0}(t) \\ \hat{\mathbf{W}}_{s,\frac{\pi}{2}}(t) \end{bmatrix} \quad (78)$$

where

$$\mathbf{J}_{\mathbf{q}} = \begin{bmatrix} \Re(\mathbf{U}_+) & -\Im(\mathbf{U}_+) \\ \Im(\mathbf{U}_-) & \Re(\mathbf{U}_-) \end{bmatrix} \quad (79)$$

is a Jacobian block matrix of order $2K$, the K -dimensional matrices \mathbf{U}_{\pm} are explicitly defined through their complex-valued components

$$\mathbf{U}_{\pm,l,p} = (\mathcal{R}_{l,p} - \mathcal{R}_{l,-p}) \pm (\mathcal{S}_{l,p} - \mathcal{S}_{l,-p})^* \quad (80)$$

with $l, p \in \{1, \dots, K\}$, while the K -dimensional vacuum noise operators $\hat{\mathbf{W}}_{s,0}(t)$ and $\hat{\mathbf{W}}_{s,\frac{\pi}{2}}(t)$ are explicitly defined as

$$\begin{aligned} \hat{\mathbf{W}}_{s,0}(t) &= \frac{1}{\sqrt{2}} \begin{bmatrix} \hat{\mathbf{V}}_{s,+1}(t) - \hat{\mathbf{V}}_{s,-1}(t) \\ \vdots \\ \hat{\mathbf{V}}_{s,+L}(t) - \hat{\mathbf{V}}_{s,-L}(t) \end{bmatrix} + \text{H. c.} \quad (81) \\ \hat{\mathbf{W}}_{s,\frac{\pi}{2}}(t) &= -\frac{i}{\sqrt{2}} \begin{bmatrix} \hat{\mathbf{V}}_{s,+1}(t) - \hat{\mathbf{V}}_{s,-1}(t) \\ \vdots \\ \hat{\mathbf{V}}_{s,+L}(t) - \hat{\mathbf{V}}_{s,-L}(t) \end{bmatrix} + \text{H. c.} \end{aligned}$$

It is interesting to note that the Jacobian matrix $\mathbf{J}_{\mathbf{q}}$ is real-valued, as it is built with the real and imaginary parts of the complex-valued matrices \mathbf{U}_{\pm} . This Jacobian is generally *not* diagonal, meaning that in a Kerr comb, all these quadratures are coupled.

Equations (42) and (75) allow to determine the output vectorial quadratures following

$$\begin{bmatrix} \delta \hat{\mathbf{Q}}_{\text{out},0}(t) \\ \delta \hat{\mathbf{Q}}_{\text{out},\frac{\pi}{2}}(t) \end{bmatrix} = \sqrt{2\kappa_r} \begin{bmatrix} \delta \hat{\mathbf{q}}_0(t) \\ \delta \hat{\mathbf{q}}_{\frac{\pi}{2}}(t) \end{bmatrix} - \begin{bmatrix} \hat{\mathbf{W}}_{r,0}(t) \\ \hat{\mathbf{W}}_{r,\frac{\pi}{2}}(t) \end{bmatrix}. \quad (82)$$

The time-domain dynamics of the generic quadrature $\delta \hat{\mathbf{q}}_{\varphi}$, as well as its output counterpart $\delta \hat{\mathbf{Q}}_{\text{out},\varphi}$ are determined by combining the above equation with Eq. (76).

C. Correlations and squeezing spectra

The Fourier spectra of the output signals can be determined using the output correlation matrix. After translating Eqs. (78) and (82) in the Fourier domain, the Fourier spectrum of the output vectorial quadrature is found to be equal to

$$\begin{aligned} \begin{bmatrix} \delta \tilde{\mathbf{Q}}_{\text{out},0}(\omega) \\ \delta \tilde{\mathbf{Q}}_{\text{out},\frac{\pi}{2}}(\omega) \end{bmatrix} &= -\sqrt{2\kappa_r} [\mathbf{J}_{\mathbf{q}} + i\omega \mathbf{I}]^{-1} \\ &\times \sum_s \sqrt{2\kappa_s} \begin{bmatrix} \tilde{\mathbf{W}}_{s,0}(\omega) \\ \tilde{\mathbf{W}}_{s,\frac{\pi}{2}}(\omega) \end{bmatrix} \\ &- \begin{bmatrix} \tilde{\mathbf{W}}_{r,0}(\omega) \\ \tilde{\mathbf{W}}_{r,\frac{\pi}{2}}(\omega) \end{bmatrix}. \quad (83) \end{aligned}$$

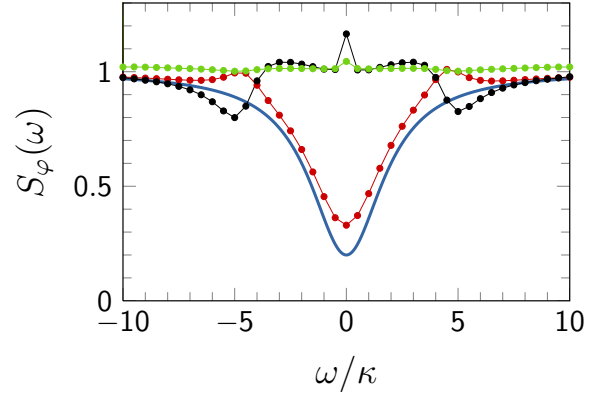


FIG. 5: (Color online) Spectra of amplitude quadratures for different mode of order $\pm kL$ in a primary comb of a roll pattern. The parameters of the system are the same as in Fig. 3(c) [with $P = 1.5 P_{\text{th}}$ and $L = 22$], except the detuning $\delta\Phi = 0.03$ that has been applied to all mode quadratures. The solid blue line is the ideal amplitude squeezing spectrum obtained from Eq. (93). The dots stand for the numerical spectra obtained with Eq. (87) [53]. Red: modes $\pm L$; Black: modes $\pm 2L$; Green: modes $\pm 3L$.

We can use the above equation to determine the $2K$ -dimensional output correlation matrix, following

$$\begin{aligned} \mathbf{C}^{\text{out}}(\omega) &= \int_{-\infty}^{+\infty} d\omega' \left\langle \begin{bmatrix} \delta \tilde{\mathbf{Q}}_{\text{out},0}(\omega) \\ \delta \tilde{\mathbf{Q}}_{\text{out},\frac{\pi}{2}}(\omega) \end{bmatrix} \begin{bmatrix} \delta \tilde{\mathbf{Q}}_{\text{out},0}(\omega') \\ \delta \tilde{\mathbf{Q}}_{\text{out},\frac{\pi}{2}}(\omega') \end{bmatrix}^{\text{T}} \right\rangle \\ &= \{2\kappa\rho[\mathbf{J}_{\mathbf{q}} + i\omega\mathbf{I}]^{-1} + \mathbf{I}\} \mathbf{C}^{\text{in}}(\omega) \\ &\times \{2\kappa\rho[\mathbf{J}_{\mathbf{q}} - i\omega\mathbf{I}]^{-1} + \mathbf{I}\}^{\text{T}} \\ &+ 4\kappa^2\rho(1-\rho) \{[\mathbf{J}_{\mathbf{q}} + i\omega\mathbf{I}]^{-1}\} \mathbf{C}^{\text{in}}(\omega) \\ &\times \{[\mathbf{J}_{\mathbf{q}} - i\omega\mathbf{I}]^{-1}\}^{\text{T}}, \quad (84) \end{aligned}$$

where ρ is the squeezing parameter defined in Eq. (63), and $\mathbf{C}^{\text{in}}(\omega)$ is the $2K$ -dimensional input correlation matrix

$$\begin{aligned} \mathbf{C}^{\text{in}}(\omega) &= \int_{-\infty}^{+\infty} d\omega' \left\langle \begin{bmatrix} \tilde{\mathbf{W}}_{s,0}(\omega) \\ \tilde{\mathbf{W}}_{s,\frac{\pi}{2}}(\omega) \end{bmatrix} \begin{bmatrix} \tilde{\mathbf{W}}_{s,0}(\omega') \\ \tilde{\mathbf{W}}_{s,\frac{\pi}{2}}(\omega') \end{bmatrix}^{\text{T}} \right\rangle \\ &= \begin{bmatrix} \mathbf{I} & i\mathbf{I} \\ -i\mathbf{I} & \mathbf{I} \end{bmatrix} \quad (85) \end{aligned}$$

where \mathbf{I} is the K -dimensional identity matrix. It is interesting to note that this input correlation matrix is found to be frequency independent.

For each sidemode pair $\pm l$, the quadrature spectra are explicitly defined as

$$\begin{aligned} S_{\varphi,l}(\omega) &= \mathcal{C}_{11;(l,l)}^{\text{out}} \cos^2 \varphi + \mathcal{C}_{22;(l,l)}^{\text{out}} \cos^2 \varphi \\ &+ [\mathcal{C}_{12;(l,l)}^{\text{out}} + \mathcal{C}_{21;(l,l)}^{\text{out}}] \cos \varphi \sin \varphi \quad (86) \end{aligned}$$

where the coefficients are complex-valued coefficients $\mathcal{C}_{ab;(l,l)}^{\text{out}}$ with $a, b \in \{1, 2\}$ are diagonal elements of the

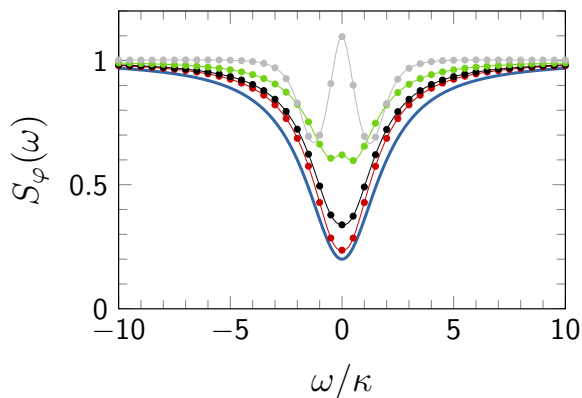


FIG. 6: (Color online) Spectra of amplitude quadratures for different mode of orders $\pm l$ of the comb from a isolated bright soliton. The power is set to $P = 4$ mW, and $\sigma = -2\kappa$. The same offset $\delta\Phi = \frac{\pi}{2} - 0.04$ has been applied to all mode quadratures. The solid blue line is the ideal amplitude squeezing spectrum obtained from Eq. (93). The dots stand for the numerical spectra obtained with Eq. (87) [53]. Red: $l \pm 1$; Black: $l \pm 5$; Green: $l \pm 10$. Gray: $l \pm 20$.

K -dimensional matrices $\mathbf{C}_{ab}^{\text{out}}(\omega)$ that are used to write $\mathbf{C}^{\text{out}}(\omega)$ in Eq. (84) under the form of the block matrix

$$\mathbf{C}^{\text{out}}(\omega) = \begin{bmatrix} \mathbf{C}_{11}^{\text{out}}(\omega) & \mathbf{C}_{12}^{\text{out}}(\omega) \\ \mathbf{C}_{21}^{\text{out}}(\omega) & \mathbf{C}_{22}^{\text{out}}(\omega) \end{bmatrix}. \quad (87)$$

The analytical expression of provided by Eq. (87) allows to plot the spectra of any quadrature for any pair of sidemodes $\pm l$, regardless of the size of the Kerr comb.

In the next two sections, we investigate in more detail the squeezing phenomena that can take place in Kerr combs originating from roll patterns and from solitons. For all our simulations, we will consider a calcium fluoride (CaF_2) resonator with main radius $a = 2.5$ mm, and pumped around 1550 nm in the add-through configuration. The intrinsic and extrinsic Q -factors are fixed to $Q_{\text{int}} \equiv Q_i = 10^9$ and $Q_{\text{ext}} \equiv Q_t = 0.25 \times 10^9$, respectively, yielding loaded quality factor $Q_{\text{tot}} = Q_t Q_i / (Q_i + Q_t) = 0.2 \times 10^9$, a full linewidth at half-maximum $2\kappa = \Omega_0 / Q_{\text{tot}} = 2\pi \times 0.97$ MHz, and a squeezing factor $\rho = Q_i / (Q_i + Q_t) = 0.8$. The group velocity index is $n_g = 1.43$, so that the free-spectral range is $\Delta\omega_{\text{FSR}} = 2\pi \times 13.35$ GHz. The nonlinear coefficient is set to $\gamma = 0.001$, corresponding to $g_0 = 2\pi \times 57.2$ μHz . For simulations in the anomalous dispersion regime (rolls and bright solitons), the overall second-order dispersion is fixed to $\beta_2 = -12.4 \times 10^{-27}$ s^2/m , which translates to $\zeta_2 = 2\pi \times 2.9$ kHz. In the normal dispersion regime (dark solitons), the dispersion parameters are set values opposite to those of the anomalous case.

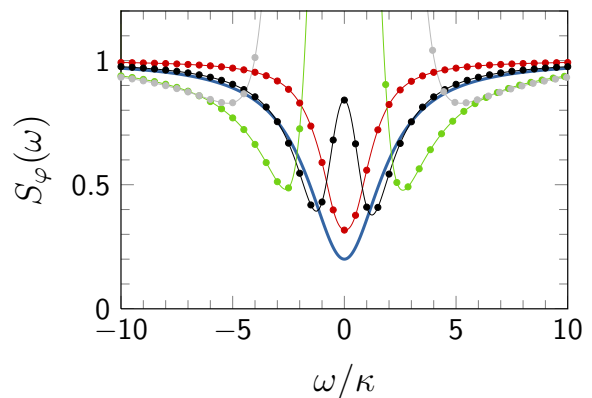


FIG. 7: (Color online) Spectra of amplitude quadratures for different mode of orders $\pm l$ of the comb from a isolated dark soliton. The power is set to $P = 5.3$ mW, and $\sigma = -2.5\kappa$. The same offset $\delta\Phi = 0.72$ has been applied to all mode quadratures. The solid blue line is the ideal amplitude squeezing spectrum obtained from Eq. (93). The dots stand for the numerical spectra obtained with Eq. (87) [53]. Red: $l \pm 1$; Black: $l \pm 5$; Green: $l \pm 10$. Gray: $l \pm 20$.

VI. QUADRATURE SQUEEZING IN ROLL PATTERNS AND SOLITONS

Rolls are azimuthal Turing patterns that emerge in the system when the resonator is pumped above a certain critical value. In the temporal domain, they are characterized by an integer number L of stationary nodes and anti-nodes of the optical energy in the azimuthal direction of the resonator. In the spectral domain, they yield a comb where only the sidemodes of order $l = \pm kL$ (k being an integer) do oscillate. These combs, which are sometimes referred to as primary combs, are particularly important because they are the most robust and stable patterns that can be obtained experimentally. Bright solitons, on the other hand, emerge in the system in the regime of anomalous dispersion, after a sub-critical bifurcation. Finally, dark solitons can be excited in the regime of normal dispersion, and in first approximation, they topologically connect the (hysteretic) upper and lower flat states inside the resonator. These various dynamical states have been investigated extensively in ref. [39]. In the forthcoming sub-sections, we will determine the squeezing spectra for the combs corresponding to all these stationary states.

A. Quadrature squeezing in roll patterns with 3 modes

In order to understand the spectra of amplitude and phase quadratures, it is important to analyze in detail the case where there are only 3 modes in the comb. As explained in Sec. IV B, such 3-modes combs emerge in the

supercritical case close to threshold, and they feature a multiplicity $L \simeq \sqrt{(2/\zeta_2)[\sigma + \Delta\omega_{\text{tot}}]}$. It is useful to recall that regardless of the initial conditions, the two sidemodes $|\mathcal{A}_{\pm L}|$ have the same amplitude and according to Eq. (73), the sum of their phases is a constant, following $\phi_L + \phi_{-L} = \text{Const} = 2\Phi_L$. Without loss of generality, we can consider in this 3-modes case that the semi-classical solutions $\mathcal{A}_{\pm L}$ have the same phase $\Phi_L \equiv \Phi$, i. e., they are considered identical. It is also noteworthy that close to threshold, the phase ϕ_0 is a constant that is independent from the sidemodes.

In this 3-modes configuration, there is only a single pair of amplitude and phase quadratures, namely $\delta\hat{q}_{0,L}$ and $\delta\hat{q}_{\frac{\pi}{2},L}$. Therefore, the matrices \mathbf{U}_{\pm} degenerate to scalars following $\mathcal{U}_{\pm} \equiv \mathcal{U}_{\pm,LL}$, yielding

$$\begin{aligned} \mathcal{U}_+ &= +2g_0\{|\mathcal{A}_L|^2 \sin\Phi + |\mathcal{A}_0|^2 \sin(2\phi_0 - \Phi)\} e^{-i\Phi} \\ \mathcal{U}_- &= -2ig_0\{|\mathcal{A}_L|^2 \cos\Phi + |\mathcal{A}_0|^2 \cos(2\phi_0 - \Phi)\} e^{-i\Phi}. \end{aligned} \quad (88)$$

Accordingly, the Jacobian matrix $\mathbf{J}_{\mathbf{q}}$ becomes 2-dimensional. Interestingly, it already appears that when the quadratures are rotated by an angle Φ , the value of \mathcal{U}_+ becomes pure real, while \mathcal{U}_- becomes pure imaginary. In other words, the quadrature $\delta\hat{q}_{\Phi,L}$ is a pure amplitude quadrature, while the quadrature $\delta\hat{q}_{\Phi+\frac{\pi}{2},L}$ corresponds to a pure phase quadrature.

Using Eqs. (74) and (78), it can be shown that the dynamics of these pure quadratures can be explicitly determined as

$$\delta\dot{\hat{q}}_{\Phi,L} = -2\kappa_a \delta\hat{q}_{\Phi,L} + \sum_s \sqrt{2\kappa_s} \hat{W}_{s,\Phi}(t) \quad (89)$$

$$\delta\dot{\hat{q}}_{\Phi+\frac{\pi}{2},L} = -2\kappa_p \delta\hat{q}_{\Phi,L} + \sum_s \sqrt{2\kappa_s} \hat{W}_{s,\Phi+\frac{\pi}{2}}(t) \quad (90)$$

where linear coefficients are

$$\kappa_a = -g_0|\mathcal{A}_0|^2 \sin(2\phi_0 - 2\Phi) \quad (91)$$

$$\kappa_p = g_0\{|\mathcal{A}_L|^2 + |\mathcal{A}_0|^2 \cos(2\phi_0 - 2\Phi)\} \quad (92)$$

while the noise driving terms are defined analogously to the quadratures of Eq. (74) using Eqs. (82). The normalized spectra corresponding to the pure amplitude and phase output quadratures can finally be calculated as

$$\begin{aligned} S_a(\omega) &= \left\langle |\delta\tilde{\mathbf{Q}}_{\text{out},\Phi}(\omega)|^2 \right\rangle \\ &= 1 - \rho \frac{4\kappa_a^2}{\omega^2 + 4\kappa_a^2} \end{aligned} \quad (93)$$

$$\begin{aligned} S_p(\omega) &= \left\langle |\delta\tilde{\mathbf{Q}}_{\text{out},\Phi+\frac{\pi}{2}}(\omega)|^2 \right\rangle \\ &= 1 + \rho \frac{4\kappa_a^2}{\omega^2} \left[1 + \frac{4\kappa_p^2}{\omega^2 + 4\kappa_a^2} \right]^2. \end{aligned} \quad (94)$$

It can be demonstrated that $\kappa_a \equiv \kappa$ in a 3-modes comb, and as a consequence, Eq. (93) becomes in fact identical

to Eq. (62). This is explained by the fact that $\delta\hat{q}_{\Phi,L}$ is a pure amplitude quadrature, which exactly corresponds to the case of photon number squeezing we have studied in Sec. IV B. On the other hand, the phase quadrature is characterized by a spectrum that is diverging at $\omega = 0$, and this divergence is a generic signature of phase noise spectra. It is noteworthy that $S_a(\omega)$ is always smaller than 1 and does not depend on the modal amplitudes, while $S_p(\omega)$ is always larger than 1, and does depend on $|\mathcal{A}_0|$ and $|\mathcal{A}_{\pm L}|$. Figure 2 displays both the amplitude (solid lines) and phase (dashed lines) quadratures for various values of the squeezing parameter ρ , when the other parameters are kept constant. As explained earlier, better squeezing is ensured when ρ gets closer to 1, which physically corresponds to strong over-coupling.

The quadratures perturbations $\delta\hat{q}_{\varphi}$ have been expressed as a linear combination of $\delta\hat{q}_0$ and $\delta\hat{q}_{\frac{\pi}{2}}$ in Eq. (76). However, after rotation by an angle Φ , they can also be expressed as a function of the pure amplitude and phase quadratures as

$$\delta\hat{q}_{\varphi,L} = \delta\hat{q}_{\Phi,L} \cos(\varphi - \Phi) + \delta\hat{q}_{\Phi+\frac{\pi}{2},L} \sin(\varphi - \Phi), \quad (95)$$

which is just another way to express the fact that we have a pure amplitude quadrature for $\varphi = \Phi$, and a pure phase quadrature for $\varphi = \Phi + \frac{\pi}{2}$. Therefore, since the quadratures with phases $\varphi \neq \Phi, \Phi + \frac{\pi}{2}$ are mixtures of pure amplitude and phase quadratures, their spectra are expected to have with intermediate characteristics. This phenomenology is displayed in Fig. 3, where the power spectra $S_{\varphi,L}(\omega)$ explicitly defined in Eq. (87) have been plotted for various values of the quadrature angle φ . The resonator is pumped very close to threshold (in excess of 1%), and in that case, the 3 modes approximation is very accurate.

It can be seen in Fig. 3 that the pure amplitude quadrature with inverted Lorentzian spectrum predicted by Eq. (93) does not exactly correspond to the angle $\varphi = \Phi$ predicted theoretically. Instead, amplitude quadrature corresponds to a slightly different angle $\varphi = \Phi + \delta\Phi \equiv \Phi_{\text{opt}}$, where the offset angle $\delta\Phi$ is generally found to be small close to threshold. When the angle of the quadrature is slightly detuned from the optimal value Φ_{opt} , the spectra maintain the inverted Lorentzian structure (like S_a) but feature a sharp divergence at zero frequency (like S_p). As the detuning is further increased, the spectra S_{φ} lose the inverted Lorentzian structure and start to converge continuously towards the phase quadrature spectra S_p , which corresponds to $\varphi = \Phi_{\text{opt}} + \frac{\pi}{2}$. A similar phenomenology has been analyzed in depth by Gatti and Mancini in ref. [27] in the context of quantum correlations in hexagonal spatial patterns.

B. Quadrature squeezing in roll patterns with more than 3 modes

When the resonator is pumped far above threshold, the primary comb grows accordingly and features an in-

creasing number of sidemodes. As analyzed in Sec. IV A, squeezing is not guaranteed anymore in the system when there are more than 3 modes involved. However, the regime of large primary combs (with 5 modes or more) is interesting for various reasons. For instance, when the system is restricted to 3 modes close to threshold, the amplitude of the sidemodes is very weak and detection can be problematic. Pumping the system far above threshold yields significantly more powerful signals. Another interesting point is that in the super-critical regime, the higher-order sidemodes ($|l| > L$) do not appear discontinuously: they are in fact always present, even though their amplitude is extremely small close to threshold. However, their effect does never completely vanish (for example, they contribute to the offset $\delta\Phi$). It is therefore pertinent to investigate systematically how the quantum correlations are affected by these higher-order sidemodes in a primary Kerr comb.

In Figure 4, we display the best squeezing spectra for the amplitude quadratures as the pump power is increased from 1.01 to 3 times the threshold for comb generation. It should be recalled that as the pump power is increased, the parametric gain bandwidth is shifted outwards, and this explains why the mode orders L increase with the pump (see refs. [14, 15, 39]). When the system is very close to threshold ($P = 1.01 P_{\text{th}}$), the 3-modes approximation holds and the numerical simulations provide results that are in quasi-perfect agreement with the theoretical prediction. As the pump power is increased, it can be seen that there is a deviation from the ideal inverted Lorentzian profile, but excellent squeezing performance is still achieved up to $P = 3 P_{\text{th}}$ where there are more than 15 oscillating modes. This results therefore shows that even in the highly multimode regime corresponding to a resonator pumped far above threshold, very efficient squeezing is still possible in Kerr combs. It is interesting to note that the spectra and the offsets $\delta\Phi$ are not invariant, as they depend on initial conditions. This is explained by the fact that the spectra depend on the Jacobian matrices $\mathbf{J}_{\mathbf{q}}$, which are built with the complex-valued modal amplitudes, and which depend themselves depend on these initial conditions.

We have also investigated the quantum correlation properties of higher-order modes in the comb originating from a roll pattern (modes of order $l = \pm kL$ with $k = 2, 3, \dots$). Figure 5 shows that the first order modes displays very good squeezing as already discussed earlier, but the spectrum of the second order modes still feature some weak squeezing in a frequency band where it seems that there is excess noise in the spectrum of the fundamental pair of sidemodes. Squeezing is numerically found to be quasi-inexistent for the third order pair, as well as for the higher orders with $k > 3$.

C. Quadrature squeezing in bright and dark solitons

An interesting open point is to determine if squeezing with symmetric pairs of sidemodes is still possible in solitons. Solitons in WGM resonators do not emerge super-critically – their amplitude can not be arbitrary small. As a consequence, they always induce combs with a large numbers of phase-locked modes.

Figure 6 displays the quadrature spectra for some modes of a Kerr comb originating from a bright soliton. It can be seen that there is a certain angle of quadrature for which the closest sidemode pair ($l = \pm 1$) features very good squeezing, of the order the ideal squeezing of the 3-modes comb. As the mode order $|l|$ is increased and the offset $\delta\Phi$, the squeezing degrades and eventually disappears beyond $|l| \sim 20$. The case of dark solitons is presented in Fig. 7, where it can be seen that as in the bright soliton case, the sidemode pair $l = \pm 1$ displays good squeezing. However, this squeezing degrades much faster as the mode order is increased while keeping the offset phase $\delta\Phi$ constant.

VII. CONCLUSION

In this article, we have investigated in detail the quantum correlations that are taking place in stationary Kerr combs driven by the quantum noise associated to vacuum fluctuations. Particular emphasis has been laid on the two principal architectures that are routinely used for Kerr comb generation, namely the add-through and the add-drop configurations. We have shown that either a canonical quantization procedure or an Hamiltonian formalism can be used to establish the quantum stochastic equations ruling the time-domain dynamics of each mode. We have provided insight in relation with the essential commutation properties between the interaction Hamiltonian and the photon numbers, which allowed to understand the physical mechanisms leading to photon number squeezing in Kerr combs. We have then explicitly defined the quantum Langevin equations ruling the fluctuations of annihilation and creation operators for each mode, regardless of the number of modes in the comb. We have shown that this perturbation flow can be reduced to a flow of lower dimension, that rules the dynamics of both amplitude and phase quadratures for each pair of sidemodes. Our analysis has shown that the reduced 3-modes model, which is valid close to threshold for roll patterns, allows for the exact determination of the spectra of the amplitude and phase quadratures. These exact analytical solutions have been found to be very good approximations even far above threshold for roll patterns. Squeezing in bright and dark solitons has also been analyzed as well, for various pairs of sidemodes. The best squeezing spectra have been shown to be relatively close to the inverted Lorentzian profile that is predicted from the reduced 3-modes model. In stationary Kerr combs

driven by quantum-noise, squeezing can therefore be obtained regardless of the spectral extension of the comb, regardless of the dynamical state, and regardless of the dispersion regime. Our results also indicate that a key parameter is the so-called squeezing factor, which is the ratio between out-coupling and total losses. Regardless of the architecture of the Kerr comb generator (add-through or add-drop), strong over-coupling has been shown to be the always the best configuration for squeezing purposes.

This work could be extended to the case where non classical light is generated through second-harmonic generation [55–57]. New bulk materials, such as aluminum nitride (AlN), allow for the efficient excitation of both the second and third order susceptibility owing to their non-centrosymmetric crystalline structure [58], and they could be interesting materials for the exploration of a wide variety of quantum optics phenomena at chip-scale.

We have assumed in our investigations that the noise was exclusively of quantum origin, and was associated with the fundamental vacuum fluctuations. At the experimental level, other sources of noise arise [59, 60] as well, and it is important to account for this technical noise in order to perform pertinent comparisons between

theory and experiments. Future work will address this issue, as well other experimental imperfections (unbalanced detection, etc.) We expect these investigations to open the way for new applications in the area of guided quantum optics at telecom wavelengths, and to provide an idoneous platform for the investigation of the fundamental properties of light at the quantum level [61, 62], in general, and for optical frequency combs in particular [63, 64].

Acknowledgements

The author would like to acknowledge financial support from the European Research Council (ERC) through the projects StG NextPhase and PoC Versyt, from the *Centre National d'Etudes Spatiales* (CNES) through the project SHYRO, from the *Région de Franche-Comté* through the project CORPS, and from the Labex ACTION. The author would also like to thank *Peyresq – Foyer d'Humanisme* in France, where a research stay has permitted to complete a significant part of this work.

-
- [1] T. J. Kippenberg, S. M. Spillane, and K. J. Vahala, *Kerr-Nonlinearity Optical Parametric Oscillation in an Ultrahigh-Q Toroid Microcavity*, *Phys. Rev. Lett.* **93**, 083904 (2004).
 - [2] A. A. Savchenkov, A. B. Matsko, D. Strekalov, M. Mohageg, V. S. Ilchenko, and L. Maleki, *Low Threshold Optical Oscillations in a Whispering Gallery Mode CaF₂ Resonator*, *Phys. Rev. Lett.* **93**, 243905 (2004).
 - [3] P. Del'Haye, A. Schliesser, A. Arcizet, R. Holzwarth, and T. J. Kippenberg, *Optical frequency comb generation from a monolithic microresonator*, *Nature* **450**, 1214 (2007).
 - [4] J. S. Levy, A. Gondarenko, M. A. Foster, A. C. Turner-Foster, A. L. Gaeta, and M. Lipson, *CMOS-compatible multiple-wavelength oscillator for on-chip optical interconnects*, *Nature Photonics* **4**, 37 (2010).
 - [5] T. J. Kippenberg, R. Holzwarth, and S. A. Diddams, *Microresonator-Based Optical Frequency Combs*, *Science* **322**, 555 (2011).
 - [6] F. Ferdous, H. Miao, D. E. Leaird, K. Srinivasan, J. Wang, L. Chen, L. T. Varghese and A. M. Weiner, *Spectral line-by-line pulse shaping of on-chip microresonator frequency combs*, *Nature Photonics* **5**, 770 (2011).
 - [7] J. Li, H. Lee, T. Chen, and K. J. Vahala, *Low-Pump-Power, Low-Phase-Noise, and Microwave to Millimeter-Wave Repetition Rate Operation in Microcombs*, *Phys. Rev. Lett.* **109**, 233901 (2012).
 - [8] P. Del'Haye, S. B. Papp, and S. A. Diddams, *Hybrid Electro-Optically Modulated Microcombs*, *Phys. Rev. Lett.* **109**, 263901 (2012).
 - [9] D. J. Moss, R. Morandotti, A. L. Gaeta, and M. Lipson, *New CMOS-compatible platforms based on silicon nitride and Hydex for nonlinear optics*, *Nature Photonics* **7**, 597 (2013).
 - [10] J. Pfeifle *et al.*, *Coherent terabit communications with microresonator Kerr frequency combs*, *Nature Phot.* **8**, 375 (2014).
 - [11] S. B. Papp, K. Beha, P. Del'Haye, F. Quinlan, H. Lee, K. J. Vahala, and S. A. Diddams, *Microresonator frequency comb optical clock*, *Optica* **1**, 10 (2014).
 - [12] P. Del'Haye, K. Beha, S. B. Papp, and S. A. Diddams, *Self-Injection Locking and Phase-Locked States in Microresonator-Based Optical Frequency Combs*, *Phys. Rev. Lett.* **112**, 043905 (2014).
 - [13] T. Herr, V. Brasch, J. D. Jost, C. Y. Wang, N. M. Kondratiev, M. L. Gorodetsky, and T. J. Kippenberg, *Temporal solitons in optical microresonators* *Nature Photon.* **8**, 145 (2014).
 - [14] Y. K. Chembo, D. V. Strekalov, and N. Yu, *Spectrum and Dynamics of Optical Frequency Combs Generated with Monolithic Whispering Gallery Mode Resonators*, *Phys. Rev. Lett.* **104**, 103902 (2010).
 - [15] Y. K. Chembo and N. Yu, *Modal expansion approach to optical-frequency-comb generation with monolithic whispering-gallery-mode resonators*, *Phys. Rev. A* **82**, 033801 (2010).
 - [16] Y. K. Chembo and N. Yu, *On the generation of octave-spanning optical frequency combs using monolithic whispering-gallery-mode microresonators*, *Opt. Lett.* **35**, 2696 (2010).
 - [17] A. B. Matsko, A. A. Savchenkov, W. Liang, V. S. Ilchenko, D. Seidel, and L. Maleki, *Mode-locked Kerr frequency combs*, *Opt. Lett.* **36**, 2845 (2011).
 - [18] Y. K. Chembo and C. R. Menyuk, *Spatiotemporal Lugiato-Lefever formalism for Kerr-comb generation in whispering-gallery-mode resonators*, *Phys. Rev. A* **87**, 053852 (2013).
 - [19] S. Coen, H. G. Randle, T. Sylvestre, and M. Erkintalo,

- Modeling of octave-spanning Kerr frequency combs using a generalized mean-field Lugiato-Lefever model*, Opt. Lett. **38**, 37 (2013).
- [20] A. Coillet, I. Balakireva, R. Henriët, K. Saleh, L. Larger, J. M. Dudley, C. R. Menyuk, and Y. K. Chembo, *Azimuthal Turing Patterns, Bright and Dark Cavity Solitons in Kerr Combs generated with Whispering-Gallery Mode Resonators*, *IEEE Photonics Journal* **5**, 6100409 (2013).
- [21] A. Coillet and Y. K. Chembo, *On the robustness of phase locking in Kerr optical frequency combs*, Opt. Lett. **39**, 1529 (2014).
- [22] A. Coillet and Y. K. Chembo, *Routes to spatiotemporal chaos in Kerr optical frequency combs*, Chaos **24**, 013313 (2014).
- [23] L. A. Lugiato and R. Lefever, *Spatial Dissipative Structures in Passive Optical Systems*, Phys. Rev. Lett. **58**, 2209 (1987).
- [24] L. A. Lugiato and F. Castelli, *Quantum Noise Reduction in a Spatial Dissipative Structure*, Phys. Rev. Lett. **68**, 3284 (1992).
- [25] R. Zambrini, M. Hoyuelos, A. Gatti, P. Colet, L. Lugiato, and M. San Miguel, *Quantum fluctuations in a continuous vectorial Kerr medium model*, Phys. Rev. A **62**, 063801 (2000).
- [26] G. Grynberg and L. Lugiato, *Quantum properties of hexagonal patterns*, Opt. Commun. **101**, 69 (1993).
- [27] A. Gatti and S. Mancini, *Spatial Correlations in Hexagons Generated via Kerr Nonlinearity*, Phys. Rev. A **65**, 013816 (2001).
- [28] A. Dutt, K. Luke, S. Manipatruni, A. L. Gaeta, P. Nussenzeig, and M. Lipson, *On-Chip Optical Squeezing*, arXiv:1309.6371v1 (2013).
- [29] A. A. Savchenkov, A. B. Matsko, W. Liang, V. S. Ilchenko, D. Seidel and L. Maleki, *Kerr combs with selectable central frequency*, Nature Photonics **5**, 293 (2011).
- [30] C. Y. Wang, T. Herr, P. Del'Haye, A. Schliesser, J. Hofer, R. Holzwarth, T. W. Haensch, N. Picqué, and T. J. Kippenberg, *Mid-infrared optical frequency combs at 2.5 μm based on crystalline microresonators*, Nature Communications **4**, 134 (2013).
- [31] M. Bloch, S. W. McLaughlin, J.-M. Merolla, and F. Patois, *Frequency-coded quantum key distribution*, Opt. Lett. **32**, 301 (2007).
- [32] L. Olislager, J. Cussey, A. T. Nguyen, P. Emplit, S. Massar, J.-M. Merolla, and K. Phan Huy, *Frequency-bin entangled photons*, Phys. Rev. A **82**, 013804 (2010).
- [33] L. Olislager, E. Woodhead, K. Phan Huy, J.-M. Merolla, P. Emplit, and S. Massar, *Creating and manipulating entangled optical qubits in the frequency domain*, Phys. Rev. A **89**, 052323 (2014).
- [34] It is important to note that the definition of well-behaved phase operators is theoretically non-trivial.
- [35] A. B. Matsko and V. S. Ilchenko, *Optical resonators with whispering gallery modes I: Basics*, IEEE J. Sel. Top. Quantum Electron. **12**, 3 (2006).
- [36] V. S. Ilchenko and A. B. Matsko, *Optical Resonators With Whispering-Gallery Modes Part II: Applications*, IEEE J. Sel. Top. Quantum Electron. **12**, 15 (2006).
- [37] A. Chiasera, Y. Dumeige, P. Féron, M. Ferrari, Y. Jestin, G. Nunzi Conti, S. Pelli, S. Soria, and G. C. Righini, *Spherical whispering-gallery-mode microresonators*, Laser Photon. Rev. **51**, 457 (2010).
- [38] A. Coillet, R. Henriët, K. P. Huy, M. Jacquot, L. Furfaro, I. Balakireva, L. Larger, and Y. K. Chembo, *Micro-wave Photonics Systems Based on Whispering-gallery-mode Resonators*, J. Vis. Exp. **78**, e50423 (2013).
- [39] C. Godey, I. V. Balakireva, A. Coillet, and Y. K. Chembo, *Stability analysis of the spatiotemporal Lugiato-Lefever model for Kerr optical frequency combs in the anomalous and normal dispersion regimes*, Phys. Rev. A **89**, 063814 (2014).
- [40] This nomenclature is not standard, but it has been adopted here for being particularly intuitive.
- [41] A. Coillet, R. Henriët, P. Salzenstein, K. Phan Huy, L. Larger, and Y. K. Chembo, *Time-domain Dynamics and Stability Analysis of Optoelectronic Oscillators based on Whispering-Gallery Mode Resonators*, IEEE J. Sel. Top. Quantum Electron. **19**, 6000112 (2013).
- [42] Y. Dumeige, S. Trebaol, L. Ghisa T. K. N. Nguyen H. Tavernier, and P. Féron, *Determination of coupling regime of high-Q resonators and optical gain of highly selective amplifiers*, J. Opt. Soc. Am. B **25**, 2073 (2008).
- [43] H.-A. Bachor and T. C. Ralph, *A Guide to Experiments in Quantum Optics*, Wiley-VCH (2004).
- [44] W. Liang, A. A. Savchenkov, A. B. Matsko, V. S. Ilchenko, D. Seidel, and L. Maleki, *Generation of near-infrared frequency combs from a MgF₂ whispering gallery mode resonator*, Opt. Lett. **36**, 2290 (2011).
- [45] C. W. Gardiner, *Quantum noise*, Springer-Verlag (1991).
- [46] G. Grynberg, A. Aspect, and C. Fabre, *Introduction to Quantum Optics. From the Semi-classical Approach to Quantized Light*, Cambridge University Press (2010).
- [47] As a notational convention, sans serif fonts are reserved to operators. All operators are in caps, except pure cavity fields. Calligraphic fonts are reserved for semi-classical complex-valued variables, and bold fonts stand for matrices and vectors of scalars or operators. The same terminology applies to photon numbers
- [48] A. B. Matsko, A. A. Savchenkov, and L. Maleki, *Normal group-velocity dispersion Kerr frequency comb*, Opt. Lett. **37**, 43 (2012).
- [49] C. Fabre, E. Giacobino, A. Heidmann, and S. Reynaud, *Noise characteristics of a non-degenerate Optical Parametric Oscillator - Application to quantum noise reduction*, J. Phys. France **50**, 1209 (1989).
- [50] A. A. Savchenkov, A. B. Matsko, V. S. Ilchenko, and L. Maleki, *Optical resonators with ten million finesse*, Opt. Express **115**, 6768 (2007).
- [51] S. B. Papp, P. Del'Haye, and S. A. Diddams, *Mechanical Control of a Microrod-Resonator Optical Frequency Comb*, Phys. Rev. X **3**, 031003 (2013).
- [52] L. Maleki, *The optoelectronic oscillator*, Nature Photonics **5**, 728 (2011).
- [53] In Figs. 4, 5, 6, and 7, the symbols are obtained numerically and they are linked with a thin line for the purpose of eye guidance only. The possibility of a divergence to infinity in seemingly continuous lines can not be ruled out, as it can be understood from Fig. 3.
- [54] P. Parra-Rivas, D. Gomila, M. A. Matias, S. Coen, and L. Gelens, *Dynamics of localized and patterned structures in the Lugiato-Lefever equation determine the stability and shape of optical frequency combs*, Phys. Rev. A **89**, 043813 (2014).
- [55] J. U. Fürst, D. V. Strekalov, D. Elser, A. Aiello, U. L. Andersen, Ch. Marquardt, and G. Leuchs, *Quantum Light from a Whispering-Gallery-Mode Disk Resonator*, Phys.

- Rev. Lett. **106**, 113901 (2011).
- [56] M. Förtsch *et al.*, *A versatile source of single photons for quantum information processing*, Nature Communications **4**, 1818 (2013).
- [57] M. Förtsch *et al.*, *Highly efficient generation of single-mode photon pairs using a crystalline whispering gallery mode resonator*, arXiv:1404.0593v1 (2014).
- [58] H. Jung, C. Xiong, K. Y. Fong, X. Zhang, and H. X. Tang, *Optical frequency comb generation from aluminum nitride microring resonator*, Opt. Lett. **38**, 2810 (2013).
- [59] A. B. Matsko, A. A. Savchenkov, N. Yu, and L. Maleki, *Whispering-gallery-mode resonators as frequency references. I. Fundamental limitations*, J. Opt. Soc. Am. B **24**, 1324 (2007).
- [60] A. A. Savchenkov, A. B. Matsko, V. S. Ilchenko, N. Yu, and L. Maleki, *Whispering-gallery-mode resonators as frequency references. II. Stabilization*, J. Opt. Soc. Am. B **24**, 2988 (2007).
- [61] C. Fabre, *Squeezed states of light*, Physics Reports **19**, 215 (1992).
- [62] B. C. Sanders, *Review of coherent entangled states*, J. Phys. A: Math. Theor. **45**, 244002 (2012).
- [63] O. Pinel, P. Jian, R. M. De Araujo, J. Feng, B. Chalopin, C. Fabre, and N. Treps, *Generation and characterization of multimode quantum frequency combs*, Phys. Rev. Lett. **108**, 083601 (2012).
- [64] J. Roslund, R. M. De Araujo, S. Jiang, C. Fabre, and N. Treps, *Wavelength-multiplexed quantum networks with ultrafast frequency combs*, Nature Photonics **8**, 113 (2013).